ISSN 2616-5767 Vol.4, Issue 1: 26-61, DOI: 10.25236/AJETS.2021.040105

Review on heat transfer enhancement of phase-change materials using expanded graphite for thermal energy storage and thermal management

Xianglei Wang[1,*], Yanfang Shi[2], Xuedong Zhai[3], Buhe Dong[4], Yunfei Wang[1], Ruifeng Wang[1], Shu Sun[1], Yupeng Hua[1]

1. Ordos Institute of Technology, Ordos 017010, China
2. Yijinhuoluo Senior Middle School, Ordos 017200, China
3. Ordos Anxintai Environmental Protection Technology Co., Ltd, Ordos 017010, China
4. Ordos City of Chinese redbud innovation Institute, Ordos 017010, China
[*]*Corresponding Author*

ABSTRACT. *Phase-change materials (PCMs) are particularly attractive for latent heat storage because they provide a high energy storage density at a constant temperature, which corresponds to the phase transition temperature of the material. Various techniques have been introduced to enhance the thermal conductivity of PCMs. Expanded graphite (EG) is a common thermal enhancer because of its high thermal conductivity, low density, and chemical inertness. This paper provides a brief introduction of several common techniques for heat transfer enhancement and EG preparation. The present review focuses on studies that examined the preparation and characterization of EG/PCM composites, as well as the simulations and applications of EG/PCM composites in thermal management and thermal energy storage systems. Solution, melt-blending, impregnation, and compression methods are used to prepare the binary system which only contains PCMs and EG. Melt-blending, hot-pressing, impregnation, polymerization, sol-gel, and piercing-solidifying incuber methods are used to prepare the ternary system, which contains PCMs, EG, and matrix. The simulation and application data confirm that EG has obvious heat transfer reinforcement effects in thermal management and thermal energy storage systems.*

KEYWORDS: *expanded graphite, phase change materials,heat transfer enhancement,latent heat, thermal energy storage*

1. Introduction

Phase-change materials (PCMs) are widely used to store thermal energy because of their high storage density and small temperature variation from storage to retrieval during phase change. PCMs have been used for various applications such as solar power utilization, active and passive cooling of electronic devices, building applications, and waste heat recovering, storage and reutilization [1–4]. Numerous review articles [5–11] have introduced candidate PCMs and their thermophysical/transport properties, encapsulations, and heat transfer enhancements. The applications and simulations of PCMs in thermal energy storage systems have also been discussed.

The application of the majority of PCMs is limited by the low thermal conductivity of these materials that suppresses the heat exchange rates. Thus, introducing highly conductive materials and thermal conductivity promoters to form composites is a reasonable solution. Thermal conductivity promoters include metal fin, metal foam, graphite foam, expanded graphite (EG), and carbon fiber. EG is the most common promoter because of its low density and cost, as well as its high-temperature and corrosion resistance. It can also easily form composites with PCMs. The present review primarily focuses on the various types of EG-based PCM composites, which have been designed using reasonable forming processes that consider the nature of the materials. Solution, melt-blending, impregnation, compression, polymerization, sol-gel, and piercing-solidifying incuber methods are used to prepare the EG-based PCM composites. The simulations and applications of EG/PCM composites in thermal management and thermal energy storage systems are also introduced.

ISSN 2616-5767 Vol.4, Issue 1: 26-61, DOI: 10.25236/AJETS.2021.040105

2. Heat transfer enhancement techniques

Several methods are used to enhance the heat transfer in latent heat thermal storage systems. Finned tubes with different configurations in thermal storage systems has been proposed by many researchers such as Abhat *et al.* [12], Morcos *et al.* [13], Padmanabhan et al. [14], Velraj *et al.*[15, 16] and Ismail *et al.* [17].

Siegel *et al.* [18] examined dispersion with high-conductivity metal particles to improve the solidification in molten salt. However, this process increased the mass of the thermal energy storage (TES) system because the metal particles had high density, and the heat transfer reinforcing effect noticeably improved when the mass percentage of the metal particles achieved a certain proportion.

Embedding the PCMs in porous materials, such as metal foams [19, 20], graphite foams [21–23], and EG [24–27] can effectively reinforce the heat transfer speed, because the unique interconnected network structures of these materials act as quick heat transfer accesses.

Fukai *et al.* added carbon brushes made of carbon fibers into PCMs [28–30]. This method involved the accurate and easy control of the volume fraction of the fibers, and the fibers with low volume fraction were entirely dispersed in the PCMs. EG [31, 32] and natural graphite powders [31] are also often used to enhance heat transfer speed of polymer-based PCMs composites.

3. Preparation of EG/PCM composites

The preparation of EG-based PCM composites is currently the most extensively examined topic in PCMs composites. In this section, the preparation of EG, binary system composites and ternary system composites are introduced.

3.1 Preparation of expanded graphite

Natural flake graphite is first converted to expandable graphite (Fig.1a) through chemical intercalation in the presence of oxidizing agents such as concentrated nitric acid, K_2CrO_7, and $KMnO_4$ [33], and inserting reagents, such as perchloric acid and concentrated sulfuric acid [33]. Then, the expandable graphite is dried in a vacuum oven at 65 °C for 24 h. The EG is then obtained by the rapid expansion and exfoliation of expandable graphite in a furnace over 900 °C for 60 s [24]. Fukushima investigated the microwave thermal exfoliation process [34], which acts as a new rapid thermal treatment to expandable graphite.

After expansion, the EG retains the graphite flake structure, but evidently produces pores with different sizes and very large specific surface area (Figs.1b–d) [35]. The EG worms have porosities as high as 99.3% and densities as low as 3 kg m^{-3} [36]. The Brunauer-Emmett-Teller surface area of the EG is measured using a N_2 absorption instrument and is found to be 30.403 m^2 g^{-1} [35]. Inagaki *et al.* classified the EG pores into three categories [37], namely, (i) large spaces among voluble worm-like EG particles, (ii) crevice-like pores on the surface of EG particle, and (iii) net-like pores inside or on the surface of EG particle.

ISSN 2616-5767 Vol.4, Issue 1: 26-61, DOI: 10.25236/AJETS.2021.040105

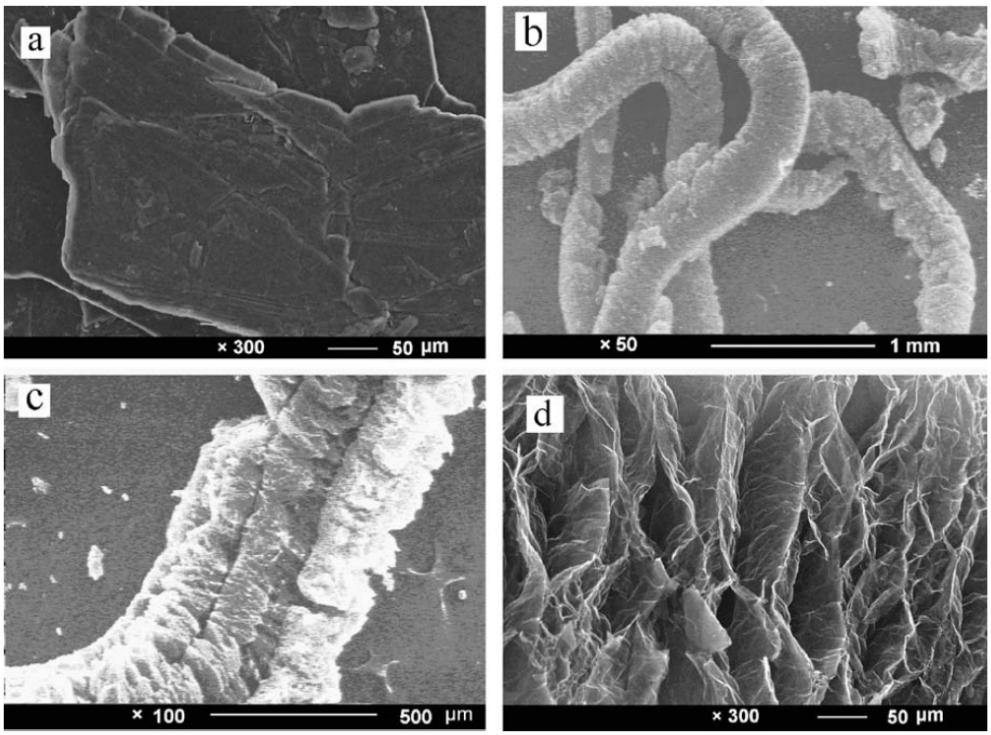

Figure.1 Scanning electron microscopy (SEM) images [35] of the (a) expandable graphite; (b) large spaces among voluble worm-like EG particles; (c) crevice-like pores on the surface of the EG particle; and (d) net-like pores inside or on the surface of the EG particle.

3.2 Preparation methods of binary system composites

Binary system composites contain only EG and PCMs. Solution, melt-bending, impregnation and compression methods are conducted under covers.

3.2.1 Solution method

The solution method can be applied to PCMs with high melting points, such as salts [38–42], or high melt viscosity, such as polyethylene glycol (PEG) [43], tetradecanol (TD) [44], using volatile solvents [43]. Common volatile solvents include deionized water [38–42], ethanol [43, 44], xylene [45], etc.

Xiao *et al.* reported the following fabrication process [38]. The molten salts made of potassium nitrate and sodium nitrate were dissolved in deionized water in a beaker. Then, EG was slowly added into the previous solution under continuous stirring at different mass rates. After EG was soaked into the solution, the solution was stirred using a strong ultrasonic homogeneous instrument for 1 h. Then, the beaker was dried in a drying oven at 100 °C for 24 h. The sample was obtained by grinding the dried PCM composite. The EG flakes were well dispersed in eutectic crystal with foliated and angular structure (Fig. 2a). The $NaNO_3$-$LiNO_3$ binary molten salts were usually adopted aqueous solution method to prepare EG-based PCM composites [40–42]. In addition, EG/$LiNO_3$-KCl [41]，EG/$LiNO_3$-NaCl [41] and EG/LiCl-NaCl [39] , EG/Alum [120] composites were also prepared using similar methods.

Both PEG and TD can be dissolved in absolute ethanol. And paraffin can be dissolved in xylenes. Based on this characteristic, Wang *et al.* [43] and Kang *et al.* [46], Xiang *et al.* [45], and Zeng *et al.* [44] prepared EG/PEG, EG/paraffin and EG/TD composites using the organic solution method, respectively.

ISSN 2616-5767 Vol.4, Issue 1: 26-61, DOI: 10.25236/AJETS.2021.040105

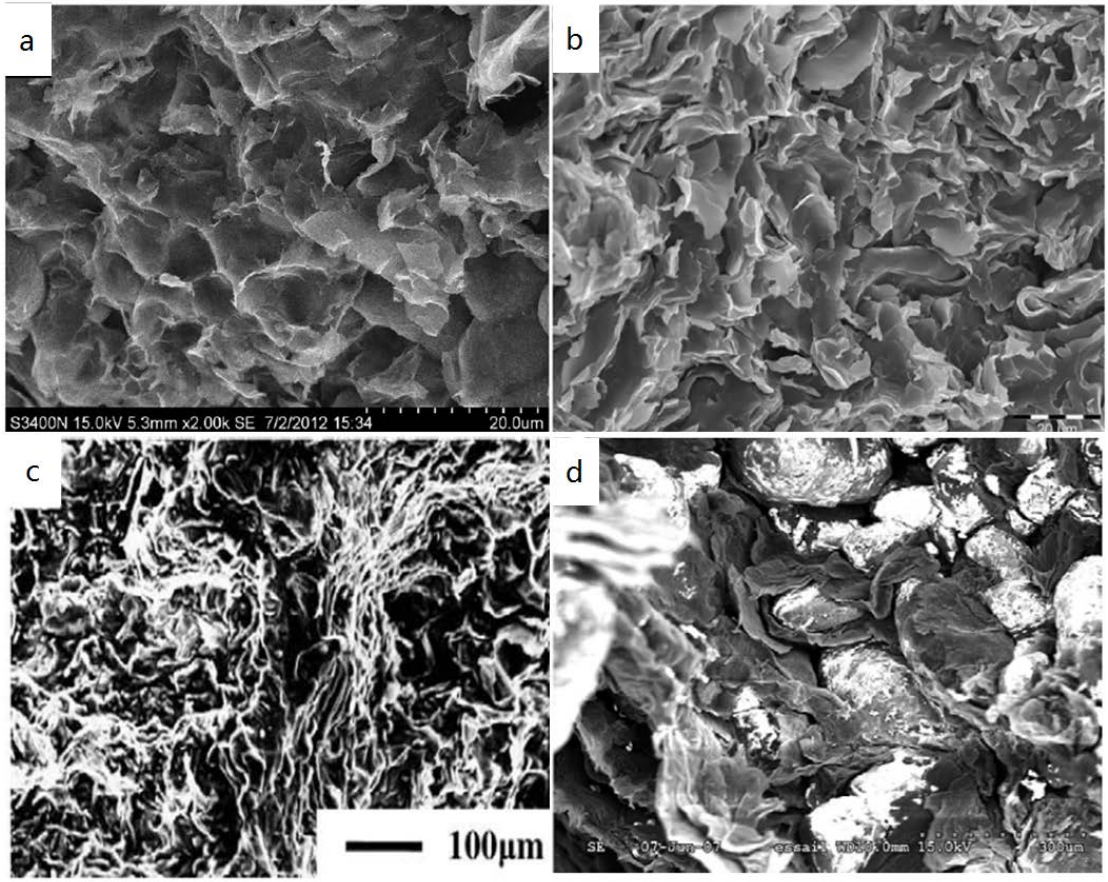

Figure. 2 SEM images of (a) EG/molten salt (2 wt% EG) [38] by solution method; (b) EG/paraffin (2 wt% EG–gold coating) [54] by melt blending method; (c) CENG/paraffin (CENG, 0.07 g cm-3) [69] by impregnation method; (d) EG/molten salt [72] by uni-axial cold-compression route.

3.2.2 Melt-blending method

The EG has a large specific surface area, high porosity, high wetting capability and high adsorption activity. Thus, the majority of EG/PCM composites are prepared based on the physical adsorption principle. Solution, melt-blending and impregnation methods are classified under the physical adsorption category.

PCMs are heated above their specific upper melting temperatures. The PCMs are then impregnated into EGs with different mass fractions and stirred using mixing equipment, such as roller mixer [35, 47, 48], magnetic stirrer [49–51] and intensive ultrasonic homogenizer [52] to ensure uniform mixing. After filtration and drying, the EG/PCM composites are obtained. Paraffin [35, 50, 52–57] and non-paraffin [47, 49, 51] organic PCMs are usually applied to form EG/PCM composites. The dispersions of the EG nanoplatelet in the organic PCMs are uniform, that is, organic PCMs was covered slightly on the EG nanoplatelet surface. EG is difficult to incorporate with molten salts using melt-blending method [36].

Xia *et al.* [47] reported that when the EG loading was less than 10 wt%, acetamide (AC) was not fully absorbed by EG, and the stability of the composite was not desirable after a few successive melting/freezing cycles. However, AC was fully impregnated into the EG when the EG mass fraction was increased to 10 wt%, which assured long-term stability. And the similar conclusion that EG mass fraction was less than 10%, $LiNO_3$-KCl could not be fully impregnated into EG, and the composites would suffer salt leakage after a few melting/solidification cycles was reported by Huang *et al.* [48]. Hu *et al.* [53] showed that the adsorption capacity of EG to paraffin is up to 92 wt%. Xia *et al.* [35] reported that when the EG mass fraction was below 5 wt%, the EG particles were in a saturated state, and the paraffin that was not fully absorbed by EG was deposited at the bottom of the container. An ultrasonic vibrator was used to uniformly mix the saturated EG with the superfluous paraffin.

ISSN 2616-5767 Vol.4, Issue 1: 26-61, DOI: 10.25236/AJETS.2021.040105

3.2.3 Impregnation method

Sari *et al.* [24, 26] reported EG/PCM composites prepared by impregnation of liquid paraffin and stearic acid (SA) into the EG with mass fractions of 2%, 4%, 7%, and 10%. Their experiments indicated that 60 min was sufficient to reach the maximum saturation level of EG with liquid paraffin. Zhang *et al.* [58–60] prepared EG/fatty acids which composited of two or three kinds of fatty acids based on the theoretical mass ratios of binary or ternary eutectic mixtures calculated via the corresponding formula PCM composites. Common fatty acids include palmitic acid (PA), capric acid (CA), myristic acid (MA), lauric acid (LA), and SA. The optimum absorption mass ratio of EG/fatty acids composites was determined as fatty acids: EG=13:1. Except natural immersion method, vacuum impregnation method was used to prepare EG-based PCM composites [61–64].

Without the use of any binding material, the EG can be compacted into various shapes to form a stable graphite matrix because of the mechanical interlocking of the particles [65]. Py *et al.* [66] first proposed supported PCMs made of paraffin impregnated by capillary forces in a compressed expanded natural graphite (CENG) matrix with bulk densities ranging from 50 kg m^{-3} to 350 kg m^{-3}. The lower density value was linked to the limit of mechanical strength of the matrix and the higher density value of permeability as well as the available porosity at which impregnation kinetics and PCMs capacity started to become too low. Mills *et al.* [67] studied the paraffin saturation curves for various EG matrix bulk densities for the small samples (in Fig. 3). The initial slope of the saturation curve decreases for higher bulk densities. This behavior indicates that low bulk density allows the PCM to quickly penetrate into the matrix, whereas a high bulk density impedes the impregnation of PCM. Zhao *et al.* [28, 68] prepared CENG/paraffin and CENG/PEG composites in a water bath at 100 °C under 0.02MPa for 3 h.

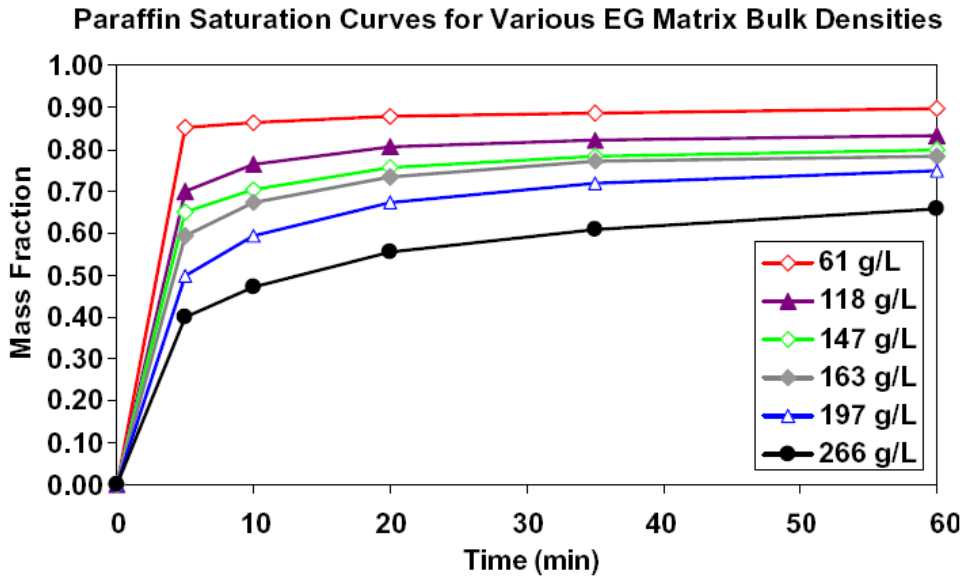

Figure. 3 Typical saturation curves for PCM impregnation [67].

Zhong *et al.* [69] first used vacuum infiltration in the preparation of CENG/paraffin composites to reduce impregnation time and enhance the porosity filling rate. The SEM image of the composites (shown in Fig. 2c) indicates that the interfaces of the two phases (paraffin wax and graphite) combine compactly because of the high wetting ability of the paraffin wax. Zhong *et al.* [70] first prepared CENG/metal alloys composites by adopting wood's alloy with low melting point. The author [71] first prepared solid-solid PCM composite-EG/neopentyl glycol (NPG) using vacuum infiltration without liquid leakage in the phase transformation process.

Pincemin *et al.* [36] tried to prepare EG/molten salt composites using high- pressure impregnation with 15 bar argon pressure. However, even after extended infiltration time of 15 h, the residual pore volume was still approximately 40%. Thus, infiltration is inefficient in preparing EG/molten salt composites in the laboratory and industrial scales.

ISSN 2616-5767 Vol.4, Issue 1: 26-61, DOI: 10.25236/AJETS.2021.040105

3.2.4 Compression method

Melt-blending and impregnation methods are not suitable for the preparation of EG/molten salt composites. Thus, compression method has been developed to resolve the previously disadvantages. The eutectic system, $NaNO_3$-KNO_3 [36, 72, 73] has been considered as the primary research subject because of its low cost, corrosiveness and environment.

This two-step elaboration route involves the following [36]. First, the solid PCMs and EG powders are physically mixed together. Then, the mixture is compressed in a mold under pressure. All operations are performed at room temperature. This elaboration route presents major advantages, namely, thermal energy is not required during elaboration, absence of corrosion effect on the equipment, and less safety procedures.

Uni-axial compression leads to a cohesive matrix made of graphite, the porosity of which is partially occupied by salt grains. At the macroscopic scale, these materials show a parallel-layered structure with alternate graphite and salt-dominant layers [72]. Within the salt-dominant layers, a random mixture of salt grains and more or less deformed EG particles is observed (Fig. 2d). Isostatic compression leads to a random distribution of salt spheres within a continuous and homogeneous matrix at the macroscopic scale.

Wang *et al.* [74] reported that the EG/sebacic acid composites with the sebacic acid mass percentage of 85% which were prepared by using impregnation method were compressed into cylinders with certain sizes and densities by dry pressing. And the preparation of EG/RT44HC [75] and EG/Microencapsulated PCM composites [119] was adopted the similar method.

3.3 Preparation methods of ternary system composites

Ternary system composites contain EG, PCMs, supporting materials and other assistant components such as a flame retardant. Melt bending, hot-pressing, impregnation, polymerization, sol-gel, and piercing-solidifying incuber methods the other methods are conducted under covers.

3.3.1 Melt-blending method

The melt-blending method in this study is also somewhat different from the aforementioned melt-blending method. Here, supporting materials fall into three categories. The first category supporting materials are usually polymer compounds, such as high density polyethylene (HDPE), low density polyethylene (LDPE), ethylene vinyl acetale (EVA), olefin block copolymer (OBC), epoxy resin (ER) and poly (styrene-butadiene-styrene). They have low melting temperature, but their melting temperature is higher than PCMs'. And supporting materials and PCMs can be soluble with each other to form an interconnected, homogeneous network system when they are heated above the melting temperature of supporting materials.

Paraffin remains as the hotspot in this field because of its low cost and high storage energy. HDPE and paraffin molecules have similar basic -CH_2- (methylene) chain configuration. Therefore, based on the principle of the dissolution in similar material structures, HDPE and paraffin can be integrated under stirring and melting conditions. Inaba *et al.* [76] first prepared form-stable paraffin/HDPE composites using melt blending. The paraffin remained in the liquid state, but HDPE solidified because the temperature of the shape-stabilized paraffin as a compound was lower than the crystallizing temperature of HDPE and greater than the melting temperature of the paraffin. In this state, the shape-stabilized paraffin can retain the solid shape without leakage of the liquid paraffin as a result of HDPE in solid state.

Sari *et al.* [77] first added EG to improve the thermal conductivity of form-stable paraffin/HDPE composites. Cheng *et al.* [31, 78], AlMaadeed *et al.* [79] and the author [80] studied the effects of EG contents on the enhancement of the thermal conductivity of composites. The SEM images (in Fig. 4a) indicate that paraffin and EG additives were more uniformly dispersed in the network formed by HDPE. Flame retardant PCMs [81-84] were also investigated. The flame retardant efficiency of intumescent flame retardant [81], chlorinated paraffin/antimony trioxide [82] and ammonium polyphosphate [84] could be improved by simultaneous application of EG [81].

ISSN 2616-5767 Vol.4, Issue 1: 26-61, DOI: 10.25236/AJETS.2021.040105

PCMs based on EG-filled composites of Fischer-Tropsch wax/LDPE [85], paraffin/1,3:2,4-di-(4-methyl) benzylidene sorbitol (MDBS) [86], paraffin/poly (styrene-butadiene-styrene) [87, 88], wax/EVA [89-91], paraffin/OBC [115] and paraffin/ER [117] was examined.

The second category supporting materials are usually porous materials like EG, such as diatomite [92], organic montmorillonite (OMMT) [93] and bentonite [123]. Li *et al.* [92] prepared EG-filled composites of paraffin/diatomite using melt blending method and mixtures were heated above the melting temperature of PCMs. Here, diatomite acts as supporting material to prevent leakage of melting paraffin. Composite PCMs added with EG can be considered effective heat storage medium because EG not only enhances heat transfer but also adsorbs paraffin into their porous structure. And the preparation of EG-filled composites of paraffin/OMMT composite [93] was adopted the similar method.

The third category supporting materials usually maintain the thermal cycle stability and dispersible uniformity of the composite PCMs, especially for salts [94, 95]. The sodium acetate trihydrate (SAT) composites containing EG and carboxymethyl cellulose (CMC) were prepared using melt blending method [94]. The addition of CMC (as the thickening agent) could reduce the aggregation of EG within the SAT and the well dispersed EG subsequently could improve the thermal conductivity.

3.3.2 Hot-pressing method

.Microencapsulated PCMs (MPCMs), with paraffin as their core material, has large latent heat. The polymer shell of MPCMs can prevent the seepage of the melted paraffin under the precondition of below the melting point of the polymer shell [32]. MPCMs cannot be uniformly dispersed in composites using melt-blending method because of its powder form.

Li et al. [96] reported a novel preparation method of polymer-based form-stable MPCM composites. First, wood flour and micro-mist graphite were mixed for 2 min in a high-speed mixer at low speed. Then, the diluted titanate ester coupling agent was sprayed into the blend system and stirred for 5 min at high speed. Third, the HDPE and MPCMs were added to the mixture and mixed for another 5 min at high speed. Finally, form-stable composites were prepared via a hot-press machine within the temperature range of 150 °C–170 °C with the pressure range of 8 MPa–10 MPa.

The author [32] first reported EG-based MPCM composites using wet-milling and hot-compaction methods. The MPCMs, EG, and HDPE were weighed according to the recipe and then mixed for 2 h using wet ball milling. Then, the mixtures were heated at 110 °C and hot pressed to obtain the form-stable composites. MPCM and EG are homogenously incorporated into the HDPE matrix (in Fig.4b). Few ruptured MPCM particles are found in the composites during the processing of wet milling and hot compaction.

ISSN 2616-5767 Vol.4, Issue 1: 26-61, DOI: 10.25236/AJETS.2021.040105

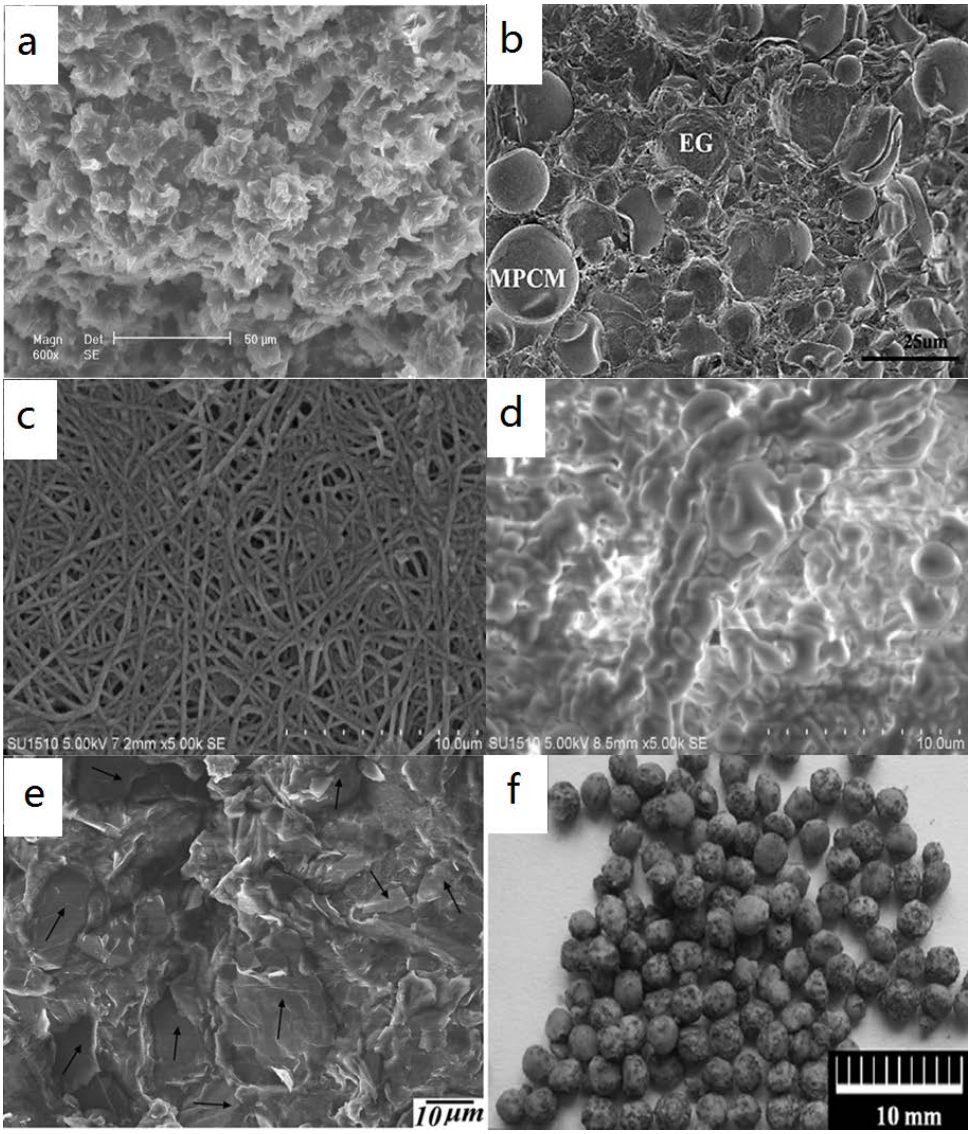

Figure. 4 SEM images of (a) EG/paraffin/HDPE (3 wt% EG) [31] by melt-blending method, (b) EG/MPCM/HDPE (20 wt% EG) [32] by hot-pressing method, (c) CA-SA/PA6 [98] by impregnation method, (d) EG/CA-SA/PA6 [98] by impregnation method, and (e) EG/PEG/PMMA (4 wt% EG) [99] by polymerization method. And optical photographs of (f) composite macrocapsules of EG/MPCMs [102] by Piercing-solidifying incuber method.

3.3.3 Impregnation method

The impregnation method in this study is also somewhat different from the aforementioned impregnation method. Here, EG according to weight percentage of supporting materials were firstly mixed in supporting materials and then immersed in molten PCMs until saturated absorption. Jeong *et al.* [97] used a vacuum impregnation method to prepare n-hexadecane and n-octadecane composites that contained sodium montmorillonite (Na-MMT) and EG, to improve the thermal conductivity of PCMs, and prevent leakage of the liquid state of PCMs. Cai *et al.* [98] prepared polyamide 6 (PA6) nanofibers and EG/PA6 composite nanofibers with 10 wt% EG using electrospinning. PA6 and EG/PA6 nanofibrous mats were immersed in molten fatty acids eutectics for 10 h until saturated absorption. As indicated in Fig. 4(c) and Fig. 4(d), the addition of EG caused the interfaces between nanofibrous mats and fatty acids of composite PCMs to become more illegible. The addition of EG might increase the porosity among fibers, and further increased physical absorption capacity of nanofubrous mats on fatty acids. The addition of EG not only increased absorption

ISSN 2616-5767 Vol.4, Issue 1: 26-61, DOI: 10.25236/AJETS.2021.040105

capacities of nanofubrous mats on eutectics but also improved thermal energy storage/retrieval rates of eutectics during phase transition.

3.3.4 Polymerization method

Polymerization is a process of reacting monomer molecules together in a chemical reaction to form polymer chains or three-dimensional networks. Here, monomer, initiator, melted PCMs, EG nanoplatelets and solvents were mixed to obtain uniform mixture under stirring for several hours at lower temperature. Then the mixtures were filtrated and washed. The clean filter was dried under vacuum at higher temperature for several hours till the monomer polymerized completely to obtain composites. EG nanoplatelets and PCMs were uniformly dispersed and embedded inside the network structure of polymer [99-100].

Zhang *et al.* [99] adopted the method of in situ polymerization upon ultrasonic irradiation, EG serving as the conductive fillers and PEG acting as the PCM were uniformly dispersed and embedded inside the network structure of polymethyl methacrylate (PMMA), which contributed to the well package and self-supporting properties of composite PCMs. As shown in Fig. 4(e), EG covered with PEG are well dispersed and enwrapped inside the PEG/PMMA matrix. The existence of EG was recognized by its uniform shape and particle size. EG/PA/polyaniline (PANI) composites were prepared using surface polymerization method by Zeng *et al.* [100].

3.3.5 Sol-gel method

The sol-gel process is a method for producing solid materials from small molecules. The process involves conversion of monomers into a colloidal solution (sol) that acts as the precursor for an integrated network (or gel) of either discrete particles or network polymers. Here, precursor, melted PCMs, EG, catalyst, and solvents were mixed to obtain uniform mixture for several hours at proper temperature. The hydrolysis and condensation reaction was preceded and the sol was obtained. The EG/paraffin/SiO_2 composites were prepared using the sol-gel method [101]. The microstructure analysis proved that the network structure of silicone gel was formed and paraffin was uniformly dispersed in the porous network. EG were also embedded in paraffin/SiO_2 composites.

3.3.6 Piercing-solidifying incuber method

Piercing-solidifying incuber method is used to prepare macrocapsules and MPCMs with high PCMs content usually using calcium alginate as matrixes and calcium chloride solution as solidification solution. Li *et al.* [102] prepared composite macrocapsules of EG/MPCMs by suspension-like polymerization followed by a piercing-solidifying incuber process. Here, MMA and 1, 4-butylenediacrylate (BDDA) were used as monomers to form the microcapsule shell. 2, 2'-azobisisobutyronitrile (AIBN) was used as initiator. And n-octadecane was used as PCM. Poly (styrene-co-maleic anhydride) sodium salt solution (19 wt%) was employed both as matrix material and dispersant for the MacroPCMs. Spherical macrocapsules could be seen in Fig .4(f). The strong polarity and increased complex crosslinking points of SMA could improve the sealing property of macrocapsules. The supercooling degree of composite macrocapsules of EG/MPCMs decreased by 3.6-4.8°C compared with that of n-octadecane bulk, by adding EG.

4. Characterization of the composite properties

4.1 Thermal conductivity enhancement

Various measurement methods, such as steady-state heat flow [36], laser flash [38], guarded heat flow meter [54], hot disk transient plane source (TPS) and transient hot-wire techniques have been used to measure the thermal conductivity of the PCM composites with the varying EG contents. A few representative composites prepared using various kinds of preparation methods are listed in Table 1.

The thermal conductivity of the composites improved evidently compared with that of pure PCM. Although the thermal conductivities vary widely depending on the preparation and measurement methods, the thermal conductivities of the composites increased obviously with EG content. The

ISSN 2616-5767 Vol.4, Issue 1: 26-61, DOI: 10.25236/AJETS.2021.040105

thermal conductivity of NaNO3-KNO3 eutectic is 0.56 W m-1 K-1 using steady-state heat flow method [36]. However, the thermal conductivity of NaNO3-KNO3 eutectic is 2.27 W m-1 K-1 using laser flash techniques [38].

The EG is an anisotropic material after mold pressing because of the stresses differences between parallel and perpendicular to the compression force direction. During compression, the direction of every graphite piece layer trends to be perpendicular to the compression force direction. For compression, the composites present anisotropic characteristics induced by the rearrangement of the graphite layers orthogonal to the compression axis. Then the radial thermal conductivity (orthogonal to the compression axis) is extensively higher than the axial one [36]. Given the anisotropic characteristics, composites with 30 wt% EG present radial thermal conductivity 92 times higher than pure eutectic, whereas composites with 20 wt% EG show radial thermal conductivity 71 times higher than pure eutectic. For impregnation, EG worms are first molded to obtain the CENG matrices, and these matrices are then impregnated in the melting PCMs. The network of the CENG matrix remains very well in the composites, which supplies a path for heat transfer. Additionally, the higher the bulk density of CENG matrix is, the denser the network is. Heat can quickly transfer through the well-developed network of the CENG matrix. The thermal conductivity of the CENG/NPG composites is improved evidently compared to that of the pure NPG [71]. This parameter is approximately 17–88 times higher than that perpendicular to the compression force and 11–26 times higher than that parallel to the compression force directions for NPG respectively. The author performed a thermal imager experiment and finite element simulation to study the heat transfer anisotropy of the composites, and the trends observed from the finite element simulation are consistent with the trends from the thermal imager [71]. The author prepared EG/MPCM/HDPE composites by first wet milling and then hot-compaction [32]. The anisotropy of the thermal conductivity could be clearly illustrated because the thin graphite nanosheets tended to be perpendicular to the compression force direction during the hot-pressing process. The thermal conductivity of the composite increased from 0.43 W m-1 K-1 to 4.59 W m-1 K-1 when 10 wt% EG was loaded. By contrast, the thermal conductivity of a composite only increased to 0.98 W m-1 K-1 when the same content of natural graphite particles was used to replace the EG. This phenomenon indicates that the physical state of thermally conductive component in the composite is highly important. The EG has much larger surface and softer than un-exfoliated graphite particles, which result in much better dispersion and tighter inter-contact of thermal active layer in MPCMs and HDPE matrix.

For the other composites using the other preparation methods, without going through compression, the EG lamellar structure is distributed homogeneously and isotropically in the composites. Thus, thermal conductivity is isotropic and its enhancement ratio is not by much.

Compared with other graphite layer-like materials, EG has a greater ability to enhance the thermal conductivity than graphene nanoplatelets (GnPs) [116] and graphite particles (GP) [32] because of its better dispersion and worm-like porous structure. An addition of 8 wt% GnPs results in 2.7-fold increase in the thermal conductivity compared to that of PA-SA,while the 8 wt% EG increases the thermal conductivity by a factor of 15.8.

Table 1 Thermal conductivity of different PCM composites. ⊥: Perpendicular to the compression force direction; //: parallel to the compression force direction.

Composites	Preparation method	EG (wt %)	Thermal Conductivity ($W\ m^{-1}\ K^{-1}$)	Measurement Method
EG/$NaNO_3$-KNO_3 [36]	Compression method	0	0.56	Steady state heat flow method
		10	11.7⊥	
		20	40.0⊥	
		30	51.5⊥	
EG/$NaNO_3$-KNO_3 [38]	Solution method	0	2.27	Laser flash technique
		0.5	2.88	
		1	3.34	
		1.5	4.14	
		2	4.89	
EG/$LiNO_3$-	Solution	0	0.84	Hot disk TPS

ISSN 2616-5767 Vol.4, Issue 1: 26-61, DOI: 10.25236/AJETS.2021.040105

$NaNO_3$ [41]	method	18.2	6.61	method
EG/paraffin [54]	Melt blending method	0	0.26	Guarded heat flow meter method
		7	0.8	
EG/AC [47]	Melt blending method	0	0.43	Transient hot-wire method
		10	2.61	
EG/MA-PA-SA [51]	Melt blending method	0	0.25	Hot disk TPS method
		7.14	2.51	
EG/paraffin [24]	Impregnated Method (non-mould)	0	0.22	Transient hot-wire method
		2	0.40	
		4	0.52	
		7	0.68	
		10	0.82	
CENG/NPG [71]	Impregnated Method (mould)	0	0.42	Laser flash technique
		10	7.3 ⊥ ,4.6//	
		13	14.2 ⊥ ,7.1//	
		18	25.0 ⊥ ,10.3//	
		24	29.0 ⊥ ,11.2//	
		29	37.6 ⊥ ,9.0//	
EG/paraffin/HDPE [31]	Melt blending method	0	0.31	Hot disk TPS method
		1	0.58	
		2	0.76	
		3	1.03	
		4	1.25	
		4.6	1.36	
EG/MPCM/HDPE [32]	Hot-pressing method	0	0.43	Laser flash technique
		5	0.94 ⊥ ,0.65//	
		10	4.59 ⊥ ,1.02//	
		15	6.01 ⊥ ,1.63//	
		20	9.89 ⊥ ,2.77//	
EG/n-hexadecane /Na-MMT [97]	Impregnation method	0	0.48	Modified TPS method
		3.67	1.11	
EG/PEG/PMMA [99]	Polymerization method	0	0.25	Hot disk TPS method
		8	2.33	
EG/PA/PANI [100]	Polymerization method	0	0.32	Steady state heat flow method
		7.87	1.08	
EG/paraffin/SiO_2 [101]	Sol-gel method	0	0.16	Hot disk TPS method
		7.2	0.25	

4.2 Thermal energy storage/retrieval properties of the EG/PCM composites

Thermal performance test was conducted in order to investigate the influences of EG on thermal energy storage/retrieval rates of composite PCMs with the experimental setup which usually includes constant temperature troughs, thermocouples, glass test tubes, a temperature data logger and a computer. PCMs without EG addition and EG/PCM composites of the same quality were separately filled into glass test tubes with the same shell thickness and diameter. Thermocouples were placed in the centers of the tubes. The test tubes were put into a constant temperature trough at constant temperatures which were higher than melting points of PCMs for thermal energy storage process. After then, they were directly subjected to retrieval process in another constant temperature trough at constant temperatures which were lower than melting points of PCMs. The transient temperature response at the center of tubes was recorded by the temperature data logger. When EG is added, the thermal response becomes more sensitive [52].

ISSN 2616-5767 Vol.4, Issue 1: 26-61, DOI: 10.25236/AJETS.2021.040105

Times for completing a heat storage and retrieval for various PCMs and EG/PCM composites are calculated from the temperature-time curve and summarized in Table 2. As can be seen from Table 2, it is obvious that both melting time and solidification time was reduced significantly for the EG/PCM composites compared with those for PCMs without EG addition. It was concluded from these results that the heat transfer rate in the EG/PCM composites were obviously higher than that in the PCMs without EG addition, which is due to the combination of the PCMs with the EG [48, 61, 98, 99, 101]. It was also concluded that composite PCMs with EG could more rapidly absorb and deliver heat supplied from a heat source compared with composite PCMs without EG addition.

Moreover, because the heat transfer rate in the heat charging process was controlled by natural convection, whereas in the heat discharging process, it was controlled by thermal conduction, the increase in the conductivity coefficient of the PCM had a more significant enhancement effect on the heat transfer in the heat release process than in the heat storage process. Therefore, the reduced time for the composite PCMs in the heat release process was more than in the heat storage process [35, 61].

The maximum temperature differences (DTmax) for EG mass fractions of 10, 20 and 30 % are determined as 8.16, 4.83 and 3.01 °C, suggesting that with higher mass content of EG, the heat transfer in the composite material would be further enhanced [48].

Table 2 The comparison of time during heat storage and retrieval between various PCMs and composites.

Composites	Preparation method	The contents of EG (%)	Temperature Range (°C)	Time required (s)
EG/paraffin [52]	Melt blending method	0	30~68	Heating 1390s Cooling 1266s
		1	30~68	Heating 970s Cooling 923s
EG/paraffin [56]	Melt blending method	3	51~27	Cooling 7200s
		6	51~27	Cooling 6000s
		9	51~27	Cooling 4080s
EG/CA [61]	Impregnated Method (non-mould)	0	30~31 30~31	Heating 5160s Cooling 3960s
		20	30~31 30~31	Heating 4260s Cooling 2260s
EG/LA [61]	Impregnated Method (non-mould)	0	40~42 40~42	Heating 3240s Cooling 3160s
		20	40~42 40~40	Heating 2520s Cooling 2140s
EG/MA [61]	Impregnated Method (non-mould)	0	50~52 50~52	Heating 4680s Cooling 3270s
		20	50~52 50~52	Heating 2310s Cooling 1440s
EG/CA-SA/PA6 [98]	Impregnated Method	0	10~31 50~23	Heating 2088s Cooling 1668s
		9.8 PA6/EG	10~31 50~23	Heating 1806s Cooling 1398s
EG/CA/PA6 [98]	Impregnated Method	0	10~33 50~29	Heating 3018s Cooling 1002s
		10 PA6/EG	10~33 50~29	Heating 2670s Cooling 852s
EG/paraffin/ diatomite [92]	Melt blending method	0	18~53 38~53	Heating 945s Heating 596s
		3	18~53 38~53	Heating 660s Heating 429s
		5	18~53 38~53	Heating 495s Heating 283s
		8	18~53 38~53	Heating 390s Heating 246s

ISSN 2616-5767 Vol.4, Issue 1: 26-61, DOI: 10.25236/AJETS.2021.040105

EG/PA-SA [58]	Impregnation method	0	18~53 75~53	Heating 750s Cooling 1740s
		7.14	18~53 75~53	Heating 210s Cooling 1080s
EG/paraffin [35]	Melt blending method	0	15~75 75~20	Heating 29400s Cooling 50100s
		7	15~75 75~20	Heating 16800s Cooling 18000s
		10	15~75 75~20	Heating15000s Cooling16800s
EG/paraffin/ OMMT [93]	Melt blending method	0 (Paraffin)	10~60	Heating 1800s
		0 (10% OMMT)	10~60	Heating 1500s
		9.76	10~60	Heating 300s
EG/paraffin [55]	Melt blending method	0	28.5~65 65~29	Heating 1040s Cooling 760s
		14.4	28.5~65 65~29	Heating 500s Cooling 240s
EG/paraffin [24]	Impregnation method	0	25.2~41.6	Heating 5460s
		4	25.2~41.6	Heating 4560s
		10	25.2~41.6	Heating 3720s
EG/paraffin/SiO_2 [101]	Sol-gel method	0(Paraffin)	12~44 44~12 27~29 29~27	Heating 3786s Cooling 5709s Melting 1263s Freezing 2403s
		0(20.8% SiO_2)	12~44 44~12 27~29 29~27	Heating 2955s Cooling 2910s Melting 690s Freezing 837s
		7.2%EG 20.8% SiO_2	12~44 44~12 27~29 29~27	Heating 1809s Cooling 1746s Melting 366s Freezing 345s
EG/SA [26]	Impregnation method	0	33~70	Heating 5700s
		2	33~70	Heating 4500s
		4	33~70	Heating 3720s
EG/$LiNO_3$-KCl [48]	Melt blending method	10	120~196	Heating 3480s
		20	120~196	Heating 2810s
		30	120~196	Heating 2460s
EG/AC[47]	Melt blending method	0	25~90 90~25	Heating 8220s Cooling 4530s
		10	25~90 90~25	Heating 8730s Cooling 1840s

4.3 Thermal properties of the EG/PCM composites

The thermal properties of the EG/PCM composites, such as phase change temperature and latent heat, were obtained using a differential scanning calorimeter (DSC) at a certain velocity under a constant stream of protective gas at a certain rate.

The latent heat values were obtained using the integral form of the DSC curve. Only a few representative composites prepared using all kinds of preparation methods are listed on Table 3.

For EG/molten salt composites, compared with pure salts, the specific latent heat of the composites is reduced by the presence of EG in a larger amount than the corresponding additional weight [36, 38]. At 20 wt% EG content, the latent heat of the composite is equal to 67.6 kJ kg^{-1}, whereas that at 30 wt% in EG content, the latent of the composite is only 42.5 kJ kg^{-1} [36]. The experimental value of latent heat is reduced by approximately 9.2% compared with the calculated data according to the mass ratio

ISSN 2616-5767 Vol.4, Issue 1: 26-61, DOI: 10.25236/AJETS.2021.040105

of the salts in the composite at only 2 wt% EG content. Comparatively, the phase transition temperatures are not significantly affected by the presence of EG. However, Huang *et al.* [48] reported that the experimental latent heat values showed an agreement with the calculated values with relative errors less than 3% for EG/$LiNO_3$-KCl composites. And the angles on melting point of EG/$LiNO_3$-KCl composites were shaper and the endothermic peaks were narrower than that of the eutectic $LiNO_3$-KCl.

For EG/organic composites, the experimental values of latent heat are consistent with the calculated values by multiplying the latent value of pure PCMs with their mass fraction with slight differences [24, 50, 71, 44, 59-60], especially for EG/paraffin with differences of less than 2% [24]. The addition of EG evidently influences on melting temperature [24, 50, 59-60]. Sari [24] reported that the onset melting temperatures of EG/paraffin composites saturated with paraffin in mass ratios of 98%, 96%, 93%, and 90% were lower than that of pure paraffin at 0.5 °C, 0.6 °C, 0.9 °C, and 1.4 °C, respectively. Zeng *et al.* [44] reported that the undercooling of PCMs composites could be diminished as EG was added. And the higher the loading of EG was, the lower the undercooling was. When the loading of EG attained 40%, the undercooling was vanished. Yuan *et al.* [59-60] reported that the supporting material EG could decrease the phase change temperature of composites. The author [71] reported that the temperature ranges between onset and peak phase-change temperatures of CENG/NPG composites decrease with increasing EG contents. Every composite exhibits a more sharp-angled phase-change peak than the pure NPG (Fig.5). The phase-change temperature of the CENG/NPG composites is slightly less than that of the pure NPG. Compared with the pure NPG, the phase-change speed of the composites accelerated because of the existence of graphite microcrystallines.

For ternary system composites, the influence of EG addition on the phase-change temperature is significant. The author reported that both solid-solid peak phase transition temperature and peak melting temperature of EG/paraffin/HDPE composites were approximately lower than paraffin/HDPE composite [80]. The author also reported that each EG/MPCM/HDPE composite exhibited a sharper and angled melting peak than the pure MPCM, and the melting peak width of the composite narrowed gradually with the increase of the mass ratio of EG. The latent heat values of the composites are slightly lower than the theoretical values calculated by multiplying the mass percentage of MPCM [32] and paraffin [80]. Cai *et al.* [98] reported that the melting point and crystallization point of PCMs composites were slightly decreased compared to fatty acids. And the addition of EG could increase physical absorption capacity of nanofibrous mats on fatty acids. Zhang *et al.* [99] also reported that the undercooling of ternary composites could be diminished as EG was added. And the higher the loading of EG was, the lower the undercooling was. It is believed that the EG additives could provide extra surfaces for the crystallization of PEG.

Table 3 Parameters of phase change temperature and latent heat of samples. Superscripts "o": onset temperature; "p": peak temperature.

Composites	Preparation method	EG (wt%)	Latent heat (kJ kg^{-1})	Phase change temperature (°C)	
EG/$NaNO_3$-KNO_3 [36]	Compression method	0	112	$222^{o,\ solid\text{-}liquid}$	
		10	80	$210^{o,\ solid\text{-}liquid}$	
		20	67.6	$223^{o,\ solid\text{-}liquid}$	
		30	42.5	$220^{o,\ solid\text{-}liquid}$	
EG/$NaNO_3$-KNO_3[38]	Solution method	0	159.46	$130.6^{p,solid\text{-}solid}$	$223.2^{p,solid\text{-}liquid}$
		0.5	148.65	$130.1^{p,solid\text{-}solid}$	$225.6^{p,solid\text{-}liquid}$
		1	147.09	$130.4^{p,solid\text{-}solid}$	$224.8^{p,solid\text{-}liquid}$
		1.5	146.81	$130.0^{p,solid\text{-}solid}$	$224.7^{p,solid\text{-}liquid}$
		2	141.91	$130.2^{p,solid\text{-}solid}$	$225.3^{p,solid\text{-}liquid}$
EG/TD [44]	Solution method	0	236.1/234.5	$35.9^{o,solid\text{-}liquid}$	$32.3^{o,liquid\text{-}solid}$
		10	198.1/196.1	$36.3^{o,solid\text{-}liquid}$	$34.8^{o,liquid\text{-}solid}$
		20	169.6/163.0	$35.9^{o,solid\text{-}liquid}$	$35.3^{o,liquid\text{-}solid}$
		30	151.2/147.2	$35.9^{o,solid\text{-}liquid}$	$35.4^{o,liquid\text{-}solid}$
		40	132.2/127.9	$35.4^{o,solid\text{-}liquid}$	$35.6^{o,liquid\text{-}solid}$
EG/$LiNO_3$-KCl [48]	Melt blending method	0	201.70	$165.6^{o,solid\text{-}liquid}$	$170.7^{p,solid\text{-}liquid}$
		10	178.10	$165.6^{o,solid\text{-}liquid}$	$169.1^{p,solid\text{-}liquid}$
		15	170.69	$165.9^{o,solid\text{-}liquid}$	$169.7^{p,solid\text{-}liquid}$
		20	164.50	$165.6^{o,solid\text{-}liquid}$	$168.6^{p,solid\text{-}liquid}$

ISSN 2616-5767 Vol.4, Issue 1: 26-61, DOI: 10.25236/AJETS.2021.040105

		25	150.96	165.6$^{o,solid-liquid}$	168.2$^{p,solid-liquid}$
		30	142.41	165.6$^{o,solid-liquid}$	168.4$^{p,solid-liquid}$
EG/n-octadecane [50]	Melt blending method	0	232.49	28.7$^{o,\ solid-liquid}$	30.3$^{p,solid-liquid}$
		9.09	207.90	27.9$^{o,\ solid-liquid}$	30.3$^{p,solid-liquid}$
		11.76	199.40	28.2$^{o,\ solid-liquid}$	30.6$^{p,solid-liquid}$
		16.67	189.52	28.1$^{o,\ solid-liquid}$	30.4$^{p,solid-liquid}$
EG/paraffin [24]	Impregnated Method (non-mould)	0	194.6	41.6$^{o,\ solid-liquid}$	
		2	192.6	41.1$^{o,\ solid-liquid}$	
		4	188.0	41.0$^{o,\ solid-liquid}$	
		7	181.9	40.7$^{o,\ solid-liquid}$	
		10	178.3	40.2$^{o,\ solid-liquid}$	
EG/CA-MA-PA [59]	Impregnated Method (non-mould)	0	135.6/131.9	18.98$^{o,solid-liquid}$	17.26$^{o,liquid-solid}$
		7.14	128.2/124.5	18.61$^{o,solid-liquid}$	16.58$^{o,liquid-solid}$
CENG/NPG [71]	Impregnated Method (mould)	0	116	39.7$^{o,\ solid-solid}$	44.6$^{p,solid-solid}$
		10	106	40.3$^{o,\ solid-solid}$	43.5$^{p,solid-solid}$
		13	100	40.7$^{o,\ solid-\ solid}$	43.9$^{p,solid-solid}$
		18	93	41.0$^{o,\ solid-\ solid}$	43.8$^{p,\ solid-solid}$
		24	82	41.1$^{o,\ solid-liquid}$	43.5$^{p,\ solid-liquid}$
		29	75	41.2$^{o,\ solid-liquid}$	43.4$^{p,\ solid-liquid}$
EG/paraffin/HDPE [80] (HDPE 35 wt%)	Melt blending method	0	124.8	48.1$^{p,\ solid-solid}$	70.0$^{p,\ solid-liquid}$
		2.5	115.8	46.8$^{p,\ solid-solid}$	67.0$^{p,\ solid-liquid}$
		5	117.8	46.8$^{p,\ solid-solid}$	65.4$^{p,\ solid-liquid}$
		7.5	112.2	47.9$^{p,\ solid-solid}$	67.2$^{p,\ solid-liquid}$
		10	101.3	48.1$^{p,\ solid-solid}$	68.1$^{p,\ solid-liquid}$
EG/paraffin/diatomite [92]	Melt blending method	0(Paraffin)	124.49	30.1$^{p,\ solid-solid}$	47.9$^{p,\ solid-liquid}$
		0 70%	109.37	30.6$^{p,\ solid-solid}$	50.7$^{p,\ solid-liquid}$
		8 Paraffin	108.13	30.0$^{p,\ solid-solid}$	52.1$^{p,\ solid-liquid}$
EG/MPCM/HDPE [32] (HDPE 40 wt%)	Hot-pressing method	0	117.4	37.1$^{o,\ solid-liquid}$	47.6$^{p,\ solid-liquid}$
		5	103.3	36.3$^{o,\ solid-liquid}$	47.5$^{p,\ solid-liquid}$
		10	84.78	37.9$^{o,\ solid-liquid}$	46.1$^{p,\ solid-liquid}$
		15	80.26	37.8$^{o,\ solid-liquid}$	44.1$^{p,\ solid-liquid}$
EG/CA-SA/PA6 [98]	Impregnated Method	0(fatty acids)	156.8/147.1	31.17$^{p,solid-liquid}$	22.94$^{p,liquid-solid}$
		0(22%PA6)	116.9/113.7	28.62$^{p,solid-liquid}$	19.40$^{p,liquid-solid}$
		9.8EG/PA6	138.5/134.3	30.38$^{p,solid-liquid}$	21.25$^{p,liquid-solid}$
EG/PMMA/PEG [99] PEG:PMMA=7:3	Polymerization method	0	120.4/104.5	45.9$^{o,\ solid-liquid}$	27.7$^{o,liquid-solid}$
		1	124.4/107.3	44.6$^{o,\ solid-liquid}$	30.3$^{o,liquid-solid}$
		2	123.8/104.7	43.4$^{o,\ solid-liquid}$	30.7$^{o,liquid-solid}$
		4	119.0/102.7	42.9$^{o,\ solid-liquid}$	31.9$^{o,liquid-solid}$
		6	116.5/99.8	42.5$^{o,\ solid-liquid}$	33.2$^{o,liquid-solid}$
		8	114.1/97.0	41.9$^{o,\ solid-liquid}$	34.6$^{o,liquid-solid}$

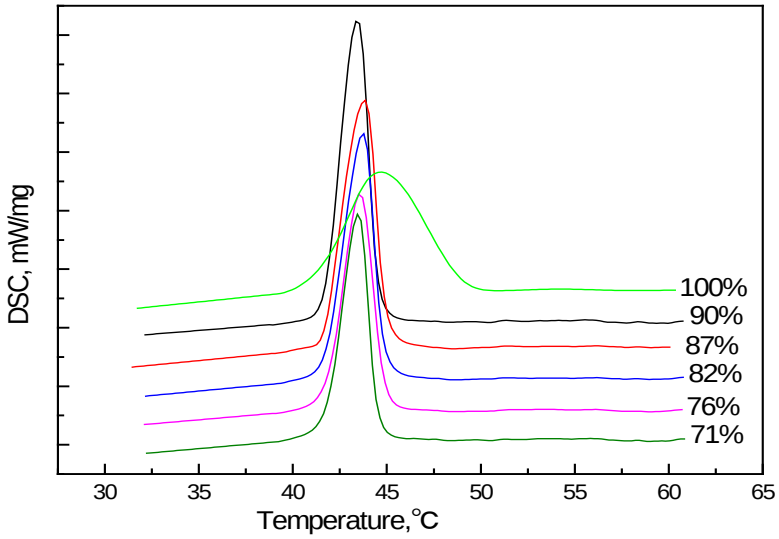

Figure 5 DSC curves of the EG/NPG composites with different NPG contents [71].

4.4 Cycle thermal stability of the EG/PCM composites

For composite PCMs, good thermal cycling stabilities over a number of thermal cycles are necessary. Thermal cycling test was performed to determine the change in the phase change temperature and latent heat of the EG/PCM composites and the results are shown in Table 4. From Table 4, organic EG/PCM composites have good thermal reliability which means a longer life cycle [51, 60, 74, 93] because EG is compatible with organic PCMs [71] and organic PCMs usually have higher viscosity compare with molten salts PCMs.

Wang *et al.* [74] reported that no obvious difference in the melting temperature was found for the EG/SA composite before and after experiencing the heating-cooling cycling test, while a slight reduction in the solidification temperature of 2.88 °C is observed. Moreover, the loss rates of latent heat of the EG/SA composites after experiencing 3000 heating-cooling cycles for melting and solidification is decreased by ca. 8.4% and 11.6% compared to the latent heat of the sample before experiencing the test, respectively. The results obtained from the 3000 heating-cooling cycling tests indicate that the EG/SA composites have good thermal reliability. Similar results were obtained by Zhang *et al.* [60].

Kao *et al.* [93] reported that the mass loss of EG/paraffin composite could be decreased by increase the content of EG after heating cycles. With the addition of OMMT, the mass loss of EG/paraffin/OMMT composite is less than that of EG/paraffin composite. It indicates that the addition of OMMT can strengthens the thermal stability of EG/paraffin composite.

For EG/molten salts composites, there are slightly larger loss of latent heat after the 100 cycles even if the content of EG is up to approximately 20%. But the phase change temperatures of the composites do not show much change either after 100 thermal cycles [41]. It shows a poor thermal stability because of leakage of salts.

Table 4 Phase change temperature change and loss rates of latent heat of samples after various thermal cycles. Superscripts "-": temperature decrease; "+": temperature increas

Composites	The contents Of EG (%)	Cycles	The loss rates of latent heat (%)		Phase change temperature change (°C)	
			melting	freezing	melting	freezing

EG/SA [74]	15	3000	8.4	11.6		-2.88
EG/MA-PA-SA[51]	7.14	500	0.59	0.40	-0.46	+1.03
		1000	1.63	1.32	0.28	+0.48
EG/LA-MA-PA[60]	5.3	50	0.88		-0.48	
EG/$LiNO_3$+KCl[41]	18.3	10	1.33	2.41	-1.1	+5.0
		40	8.10	6.60	-1.3	+6.6
		100	10.06	7.94	-1.5	+7.2
EG/$LiNO_3$+ $NaNO_3$ [41]	18.2	10	4.15	3.12	-1.6	-0.2
		40	7.65	9.8	-1.6	-0.3
		100	9.93	12.62	-1.7	-0.4
EG/ $LiNO_3$+NaCl [41]	24.2	10	4.84	9.97	-2.5	-1.4
		40	10.97	10.06	-2.7	-1.8
		100	11.71	13.32	-2.9	-2.1
EG/SAT/CMC[94]	2.5 (5%CMC)	5	2.27			
EG/paraffin/OMMT [93]	10 (0%OMMT)	50	4.02 (mass loss)			
	12.5(0%OMMT)	50	0.25 (mass loss)			
	9.76(2.44%OMMT)	50	0.03 (mass loss)			

Pincemin [36] used a SETSYS Evolution SETARAM thermobalance which is linked to a mass spectrometer, that allowed stability experiments under repeated thermal cycling in terms of potential weight loss and released gas analysis. No weight loss in the composites was observed until 350 °C after 900 h of heat treatment. Thus, the composites can be considered to be thermally stable at low temperature. The storage properties of the compounds were stable at the second cycle (after water removal) while five thermal cycles were needed to reach constant storage properties in the case of cold compressed materials (Fig.6).

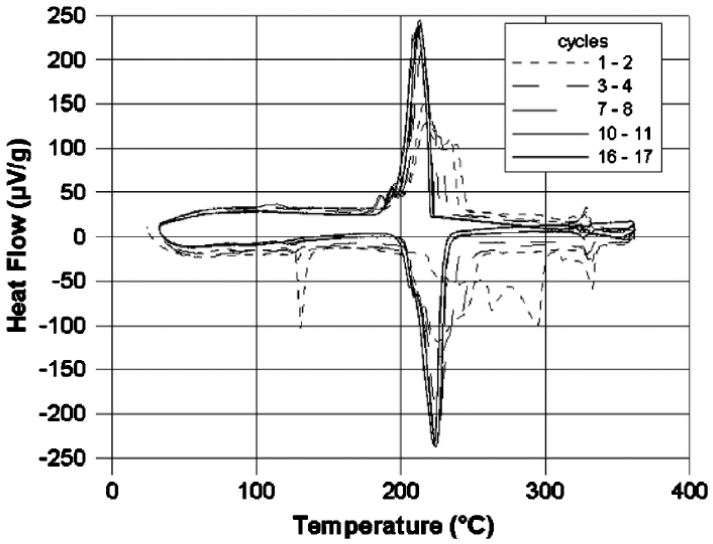

Figure 6 DSC thermal cycles of cold compressed composites ($NaNO_3$-KNO_3 eutectic with 20 wt% EG) [36].

4.5 Thermal stability properties

The thermogravimetric analyses (TGA) were performed from room temperature to high temperature at a heating rate of usually 10℃ min^{-1} under nitrogen flow. Samples ranging between 5 and 10 mg were usually sealed in an alumina pan.

The influences of EG on the thermal degradation in the PCMs are illustrated by TGA curve. The 5%, 10%, 70% weight loss temperature ($T_{5\%}$, $T_{10\%}$, and $T_{70\%}$), onset temperature of weight loss (T_{onset}), temperature of maximum decomposition (T_{max}) are calculated from TGA curves and shown in Table 5.

It is showed that thermal decomposition of PCMs gradually shifted to a higher temperature with increasing amount of EG. This indicated that the EG had positive effects on the thermal stability of the PCMs composites.

Paraffin-based ternary system composites remain as the hotspot in this field. The thermal stability of the paraffin/HDPE [79], paraffin/LDPE [85] and paraffin/EVA [89, 90] composites seem to improve in the presence of and with increasing EG content. The most probable reason for this is that (i) the interaction between the paraffin or LDPE, HDPE, EVA chains and the EG reduces the free radical chain mobility and thus slows down the degradation process, and/or (ii) the interaction between the volatile degradation products and the EG slows down the volatilization of these products. Similar conclusions were obtained for EG/PEG/PMMA composites [99]. The thermal stability of EVA and wax/EVA generally improved in the presence of EG and its combination with Cloisite 15A and diammonium phosphate (DAP) [89].

For binary system EG/PCMs composites, EG acts as supporting matrix, interacts with the PCMs and improve the overall stability of composites [45, 54, 51, 58].

Table 5 TGA results for PCMs and EG/PCM composites.

$T_{5\%}$, $T_{10\%}$, and $T_{70\%}$ are degradation temperatures at 5%, 10% and 70% mass loss, respectively. T_{onset} and T_{max} are onset temperature of weight loss and temperature of maximum decomposition, respectively.

Composites	Preparation method	EG (wt%)	T_{onset} (°C)	$T_{5\%}$ (°C)	$T_{10\%}$ (°C)	$T_{70\%}$ (°C)	T_{max} (°C)
EG/PEG/PMMA [99] PEG:PMMA=7:3	Polymerization method	0	175				
		1	180				
		2	190				
		4	198				
		6	220				
		8	215				
EG/paraffin/EVA [97] EVA:paraffin=7:3	Melt-blending method	0			260.6	456.6	
		3			286.9	481.7	
		6			287.0	480.6	
		9			288.1	484.9	
EG/paraffin/EVA [89] EVA:paraffin=3:2	Melt-blending method	0			264.2	466.2	
		6			272.7	476.7	
		6 (EG+Cloisite 15A)			312.2	476.2	
		6 (EG+DAP)			308.2	478.1	
EG/MA-PA-SA [51]	Melt blending method	0	215.7	197.1			239.8
		7.14	221.9	204.2			261.4
EG/PA-SA [58]	Impregnated Method	0	215.1	194.9			256.7
		7.14	243.7	209.3			273.3

4.6 Mechanical Properties

Mochane *et al.* [91] studied the effect of EG of mechanical properties of EVA/paraffin composites. The tensile modulus, as well as the elongation and stress at break of the blends and composites, were determined from stress–strain curves and are presented in Table 6.

The impact strength of the EG/wax/EVA composites decreased with increasing wax and graphite contents. The addition of rigid EG decreases the impact strength of the wax/EVA blends, because the EG particles act as stress concentrators for the development of cracks. Young's modulus of the wax/EVA blends increased in the presence of and with increasing EG content. This can be attributed to the high strength and aspect ratio of the graphite particles, which were smaller and a better dispersed after being covered with wax. Elongation at break of the wax/EVA blends decreased in the presence of EG content. The reason is probably that the highly crystalline, brittle wax covers the EG particles, which contributes to the easier formation and propagation of cracks under tensile forces. Better interaction between the EVA and wax covered EG may also significantly reduce the EVA chain

mobility. Irrespective of the EG content, the stress at break decreased with an increase in wax content. The main reason for this decrease is the increased amount of low molecular weight, highly crystalline wax, which deteriorates the tensile strength of the composites. Wax itself has very poor tensile properties and the wax-covered EG crystals in the amorphous phase of the EVA act as defect points for the initiation and propagation of stress cracking.

The presence of EG also increases the storage modulus of the composites, which is the result of the inherently higher storage modulus of EG and some immobilization of the EVA chains by the EG. The melting temperature of the wax in the EVA/wax/EG composite is higher than that of the wax/EVA blend. This may be attributed to the strong interaction between the wax and EG, which gave rise to restricted motion of the wax chains.

Mhike *et al.* [85] also reported that an increase in EG content increases the storage modulus of EG/paraffin/LDPE composites. And the glass transition of LDPE shifts to higher temperatures for composites because the wax crystals and EG particles in the amorphous phase of the LDPE immobilize the LDPE chains.

Zhang *et al.* [103] fabricated thermal energy storage cement mortar (TESCM) by integrating ordinary cement mortar with EG/n-octadecane composites. An increase in the mass percentage of the PCM composites results in a decrease in the compressive strengths of the TESCM cubes.

Alrashdan *et al.* [104] reported that both tensile and compressive strength increased at room temperature, but become weaker at relatively elevated temperatures with a decrease of EG content. This is somewhat different during the burst test, where it was found that as the percentage of EG decreases, the burst strength increases at room temperature.

Liu *et al.* [105] reported that when the EG content is 5%, the greatest expansion pressure increased by 25% compared with that of pure paraffin and the greatest expansion pressure can reach 87.3 MPa. It is possible to use EG/paraffin composites as driving materials.

Tao *et al.* [118] prepared ER@EG/paraffin composites according to a dual-level packaging technology. The compressive strength of PCM composites keeps a very stable value of 19.50 MPa when temperature increases from 25 to 90 °C.

Table 6 Tensile and impact properties of all the composites [91].

ε_b, σ_b and E are elongation at break, stress at break, and Young's modulus of elasticity.

Composites	EG (wt%)	Impact strength (kJ m^{-2})	σ_b (MPa)	E (MPa)	ε_b (%)
EG/paraffin/EVA [91] EVA:paraffin=7:3	0	-	7.9±0.5	92.3±20.5	114±20
	3	7.7±0.6	5.3±0.7	117±9	3.6±0.3
	6	5.8±0.7	4.7±0.3	127±9	2.5±0.2
	9	3.6±0.6	5.1±1.2	233±6	2.0±0.2
EG/paraffin/EVA [91] EVA:paraffin=3:2	0	-	4.2±0.7	66.6±6.5	46.0±9.9
	3	4.6±0.9	4.5±0.1	187±21	6.9±1.6
	6	2.8±0.0	4.5±0.5	186±16	6.3±0.4
	9	2.5±0.0	4.6±0.3	210±21	5.6±0.4
EG/paraffin/EVA [91] EVA:paraffin=1:1	0	-	6.7±0.3	72.1±14.3	37.7±13.6
	3	2.1±0.1	3.4±0.3	165±11	4.4±0.3
	6	1.9±0.1	3.8±0.7	175±11	4.8±0.4
	9	1.8±0.2	4.4±0.5	214±5	4.4±0.7

5. Simulations of EG/PCM composites systems

5.1 Phase-change heat transfer model of EG/PCM composites

Dutil *et al.* [106] reviewed the mathematical modeling and simulation of thermal energy with PCMs. The fundamental mathematical description of the phenomenon, the Stephan problem was presented. Basic mathematical descriptions were used as basis for the numerical modeling using either first or second law approaches, and fixed or adaptive meshes were provided. The problem geometry (Cartesian, spherical, and cylindrical) and specific configurations or applications (packed beds, finned surfaces, porous and fibrous materials, and slurries) were also covered.

Lu *et al.* [107] used ANSYS to simulate the phase change process of EG/paraffin composites using the heat transfer model of layered composites. The author [71] and Pincemin et al. [108] adopted the so-called effective heat capacity presented in Eq. (1) in which δ T is the temperature span variation between the beginning and the end of the transition phase, and Tm is the phase change peak temperature. The trends from the finite element simulation agree with those of the thermal imager [71]. Xia *et al.* [47] used enthalpy-porosity approach to simulate the phase change process of EG/AC composite. The results indicated good agreement between the numerical calculation and experimental results. A method based on the experiments of EG pores was proposed for constructing geometric models [123]. The calculation of a composite pore which combined 360 and 1440 pores shows that the anisotropy of effective thermal conductivity was transformed to isotropy and the effective thermal conductivity was no long changed with the increase of the number of pores, which was consistent with the macroscopic performance of this composite. Based on statistical self-similar theory, a theoretical study on the effective thermal conductivity of salt/ EG composite material is conducted by a fractal approach [124]. Multiple fractal units which can represent three-phase media were employed to describe the complex microstructures of the EG/PCM composite.

$$c_{eff} = \frac{c_{p,s} + c_{p,1}}{2} + \frac{L}{\delta T\sqrt{2\pi}} \exp\left[-\frac{\left(T_m - T_{composite}\right)^2}{\delta T^2} \right] \qquad (1)$$

5.2 Simulations of EG/PCM composites in battery thermal management (BTM) system

Passive thermal management system (TMS) using PCM with high compactness, high energy efficiency and low maintenance has drawn great attention in recent years. Passive thermal management system that used an EG/paraffin composite were designed and simulated for lithium-ion (Li-ion) battery packs [109, 110]. An electrochemistry model coupled with a thermal model was used to study the Li-ion battery cooling using EG/PCM composites [121]. Compact liquid cooling strategy with EG/PCM for Li-ion batteries were optimized using response surface methodology [122]. Andrew *et al.* [109] designed and simulated for battery packs (Fig.7) composed of six Li-ion batteries. Table 7 shows the thermo-physical properties of EG/paraffin composite, battery and battery pack used in simulations. The heat generation rate for a commercial 18650 2.2 A h Li-ion battery was experimentally measured for various constant power discharges. First, the simulation was run for each power level for a complete discharge using a minimum volume (the EG/paraffin composite filled the gaps between the circular batteries and the rectangular battery pack; total volume of Vavail = 54.16 cm^3). Table 8 shows the maximum battery temperature during the discharge for the different battery powers. The temperature of the batteries should generally not exceed 55 °C during the battery discharge. Given that the temperature of the batteries with 6.6 W battery power exceed 55 °C, the volume of the EG/paraffin composite should be increased. Table 9 shows the required volume of composite for each discharge power and the ratio of the necessary volume of EG/paraffin composite to the available volume. Results showed that for the safe operation of the battery pack during the most extreme case requires that the volume of the battery pack be almost doubled to fit sufficient PCM in the pack. Improving the properties of the PCM composite can significantly reduce the volume increase compared with the original battery pack volume. Table 10 shows the characteristics of the optimized EG/PCM composite used in this section. The results showed that a battery pack made with the improved properties will only need Vcomp =59.53 cm^3 to maintain a temperature below 55 °C during the highest discharge. The volume of the ideal composite is only 9.9% more than that available in the gaps around the batteries in the unmodified battery pack described above.

Table 7 Thermo-physical properties of EG/paraffin composite, battery and battery pack used in simulations [109].

Object	Thermal conductivity ($W\ m^{-1}\ K^{-1}$)	Specific heat ($kJ\ kg^{-1}\ K^{-1}$)	Latent heat ($kJ\ kg^{-1}$)	Bulk density ($kg\ m^{-3}$)
EG/paraffin	16.6	1.98	127	789
Battery	3	0.89	-	2670
Battery pack	0.2	1.8	-	1210
Printed circuit board	35(y), 0.35(x)	0.84	-	2000

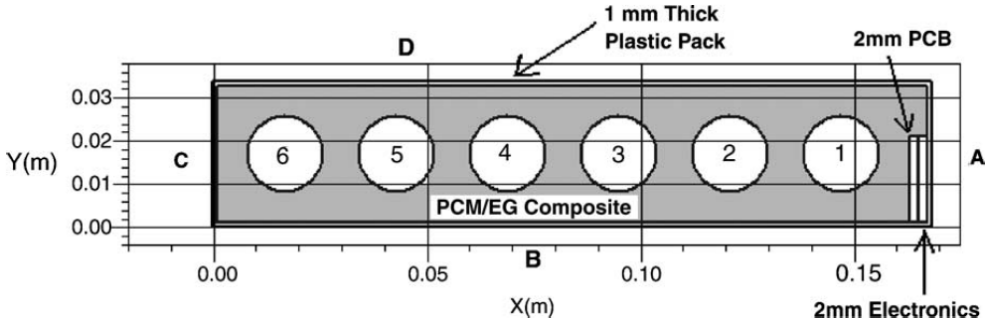

Figure 7 Schematic of battery pack used in simulations, note that the pack geometry changes for different simulations [109].

Table 8 Maximum battery temperature during discharge for minimum volume battery pack with ambient temperature of 30 °C [109].

Battery power	Total battery heat generation (W h)	Maximum battery temperature (°C)
6.6 W	0.730 (Average)	64.76
6.6 W+	0.735 (Maximum)	65.01
6.6 W-	0.725 (Minimum)	64.52
4.125 W	0.589 (Average)	54.00
4.125 W+	0.594 (Maximum)	54.24
4.125 W-	0.584 (Minimum)	53.75
2.75 W	0.322 (Average)	45.66
2.75 W+	0.324 (Maximum)	45.72
2.75 W-	0.320 (Minimum)	45.61

Table 9 Volume needed for EG/paraffin composite to maintain its temperature below 55 °C during constant power discharges with 30 °C ambient temperature [109].

Battery power	Volume of EG/ paraffin composite V_{comp} (cm^3)	Increase in volume (V_{comp}/ V_{avail})
6.6 W	105.90	1.96
6.6 W maximum	106.82	1.97
6.6 W minimum	104.97	1.94
4.125 W	78.50	1.45
4.125 W maximum	79.55	1.47
4.125 W minimum	77.45	1.43
2.75 W	29.45	0.54
2.75 W maximum	29.90	0.55
2.75 W minimum	29.00	0.54

Table 10 Ideal properties of the EG/PCM plausible with advanced manufacturing techniques [109].

Property	Value
Thermal conductivity (W $m^{-1} K^{-1}$)	25
Latent heat (kJ kg^{-1})	180
Specific heat (kJ $kg^{-1} K^{-1}$)	2.25
Bulk density of composite (kg m^{-3})	1010
Bulk density of graphite (kg m^{-3})	210

A passive thermal management system (TMS) for $LiFePO_4$ battery modules using EG/paraffin composite as the heat dissipation source to control battery temperature rise is studied using experimental and simulation by Liu *et al.* [110].

Battery pack prototype deigned (Fig.9a) and platform of the battery pack simulation model (without the PET box) (Fig.9b) is shown in Fig.9. Compared with prototype, anode/cathode tabs and differences between components, e.g., electrode, current collector and separator, were neglected for simplicity. The heat generation rate per cell during 1C-rate discharge was calculated by consisting of four parts: Joule heat, polarization heat, enthalpy change and reaction heat. Deviation between simulation and experiment is given in Fig.10. The maximum deviation is 1.95%, far less than 5%, verifying that simulation matched well with experimental results.

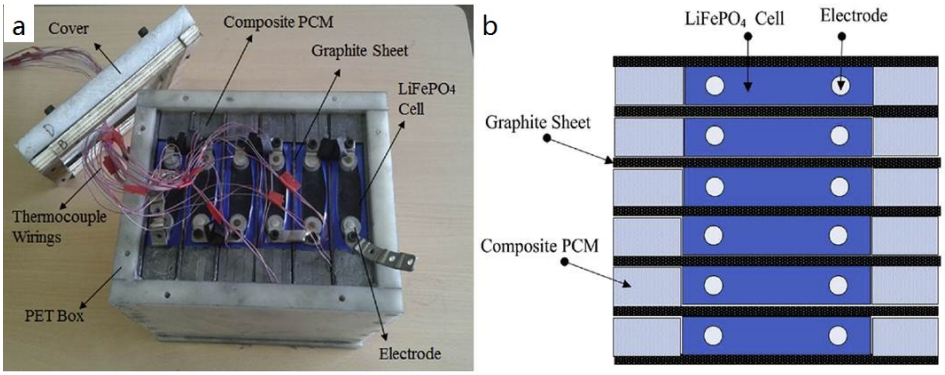

Figure 9 Battery pack prototype with the passive TMS (a). Platform of the three dimensional battery pack model (b) [110].

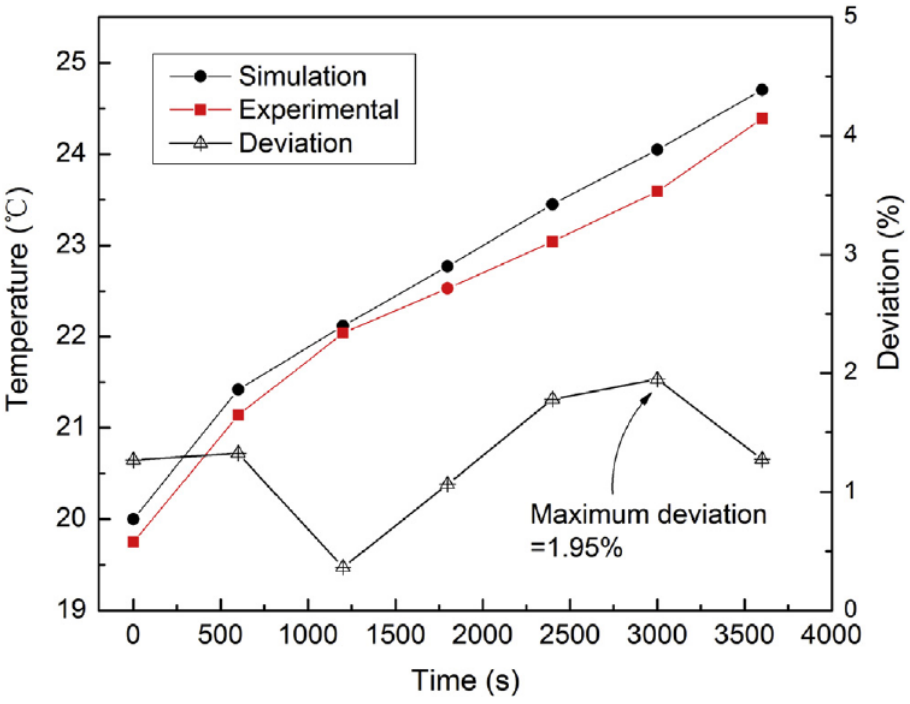

Figure 10 Comparison of temperature response of the battery module with TMS between simulation and experiment at 1C-discharge rate [110].

5.3 Simulations of EG/PCM composites in thermal energy storage

A cylindrical phase change energy storage system reported by the author [111] was modeled numerically using the finite element method. One such system is shown in Fig.11. This system composed of a cylindrical container filled with paraffin wax added copper fins or CENG/paraffin, through which a copper pipe carrying hot water was inserted. The thermophysical properties of paraffin and CENG/paraffin composites are shown in Table 11 and Table 12, respectively. The time required to reach heat equilibrium (Fig.12a) was shortened significantly by increasing the density of the CENG when it was used. The calculated results indicated that the mass ratio of CENG (1#, 0fin) to copper (paraffin, 6fins) is 1:3.82 and CENG (2#, 0fin) to copper (paraffin, 14fins) is 1:4.80. The average temperatures of CENG (1#, 0fin) and CENG (2#, 0fin) were always higher than those of copper (paraffin, 6fins) and copper (paraffin, 14fins), respectively (Fig.12b). Thus, the effect of CENG addition is more uniformly distributed in the heat transfer and more economical than adding copper fins.

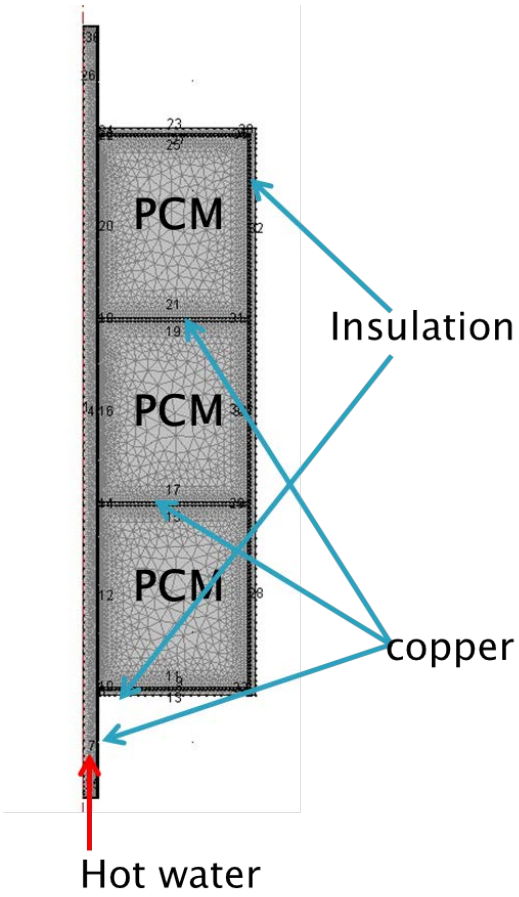

Figure 11 Physical modeling and meshing of the cylinder latent heat storage system [111].

Table 11 Thermophysical properties of paraffin wax [111].

Thermal Conductivity	0.21 W m^{-1} K^{-1}
Heat Capacity	2500J kg^{-1} K^{-1}
Enthalpy of Fusion	174 kJ kg^{-1}
Density	900 kg m^{-3}
Melting Temperature Range	310K to 316K

Table 12 Parameters of the CENG/paraffin samples [111].

Samples	Bulk density of the CENG (kg m^{-3})	Mass ratio of paraffin wax in the composites (%)	Thermal conductivity of the composites (W m^{-1} K^{-1})		Latent heat of the composites (kJ kg^{-1})
			⊥	//	
1#	70	92	10±2	9±2	144±2

2#	130	87	21±2	11±2	130±2
3#	150	83	35±2	12±2	130±2
4#	180	81	46±3	16±2	121±2
5#	260	74	66±3	17±2	120±2

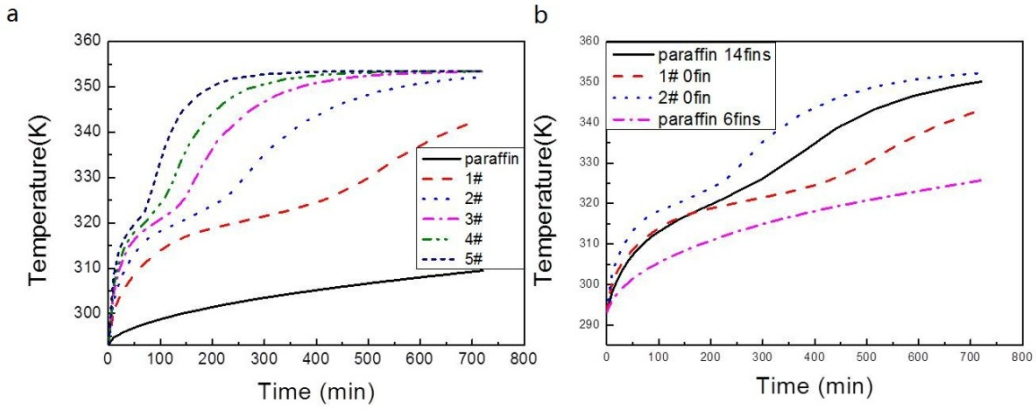

Figure 12 Average temperature variety curves of PCMs for various densities of CENG (a). Average temperature variety curves of PCMs for fins vs CENG [111].

Xia *et al.* [47] investigated the heat storage/retrieval performances of pure AC and AC/EG composite in an LTES unit experimentally and numerically. Fig.13a shows the LTES unit, consisted of a vertical stainless-steel tube, in which the PCM was enclosed. Initially, two-thirds of the test module volume was filled with the solid PCM at a room temperature of 15 °C, and the remaining space was left to accommodate volume increase in the PCM during melting. During heat storage, the temperature of the thermostatic water bath was kept at 90 °C; during heat retrieval, the water bath temperature was15-45 °C. And a 2D axisymmetric model has been compare with experimental data, as shown in Fig.13b. While modeling the melting and freezing of AC, the natural convection was taken into account, whereas for EG/AC composite, the model only involved thermal conduction. The results indicated good agreement between the numerical calculation and experimental results. Then, the model was used to interpret the thermal characteristics of the PCMs.

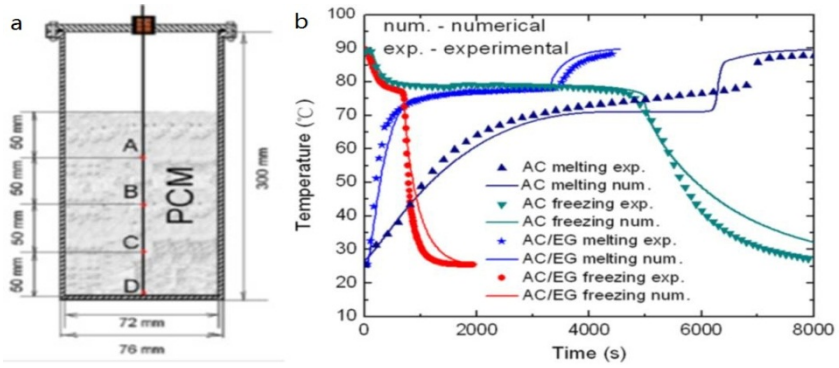

Figure 13 LTES unit and the locations of the thermocouples (a). Comparison of the numerical results and the experimental data by taking the temperature histories of point B as an example (heat storage: $T_{heating}$ =90 °C, $T_{initial}$ =25 °C and heat retrieval: $T_{cooling}$ =25 °C, $T_{initial}$ =90 °C) [47].

Luo *et al.* [112] studied the phase-change heat transfer properties of the EG/paraffin composites numerically and experimentally. The results of numerical simulation whose model is simplified as a 1D monolayer matched perfectly with those of experiment.

6. Applications of EG/PCM composites systems

6.1 Applications of EG/PCM composites in battery and chip thermal management system

As mentioned above, the effect of the passive TMS using EG/paraffin composite as the heat dissipation source on the $LiFePO_4$ battery module is studied experimentally and numerically by Liu *et al.* [110]. The cooling effect of passive TMS on the module during a mixed charge-discharge cycle and the warm-keeping effect of the passive TMS under a condition of environment temperature dropping from 30 °C to 15°C were investigated. Various battery heat dissipation module contained EG/PCMs are shown in Fig.14. Experimental curves of the modules with and without TMS during a mixed charge-discharge cycle and warm-keeping test are shown in Fig. 15a and Fig. 15b, respectively. As shown in Fig.15a, temperature of the module with PCM rose at a much smaller rate compared with the other one. In the end, the module with TMS was only 25.7 °C, and the other one was 36.8 °C, exhibiting that the battery temperature rise decreased significantly due to the presence of PCM. As shown in Fig. 15b, the temperature of the battery module with PCM dropped much more slowly compared with the module without PCM. It took 420 min for the former module when the battery temperature dropped to 20 °C, whereas the latter one lasted only 200 min for the same temperature decrease. Those experiment results demonstrate that the PCM can effectively keep the battery within an optimum operating temperature range for a long period of time.

The maximum temperatures of the battery modules with EG/paraffin [125] decreased more than 10%, 12% and 20% at 1C, 3C and 5C discharge rates, respectively, compared with pure paraffin. Ling *et al.* [126] reported that the highly thermally conductive 60 wt RT44HC/EG composite PCM can narrow the temperature variation among the cells and hence help to reduce the voltage differences. So the high thermal conductivity of the PCM plays an important role in achieving a uniform temperature distribution to improve the consistency of the battery performance.

Aluminum fins were used to couple with EG/PCM composite for optimizing the heat dissipation of the whole BTM system [127]. The as-constructed EG/PCM composite coupled with fins system presents much better heat dissipation performance than the system without fins.

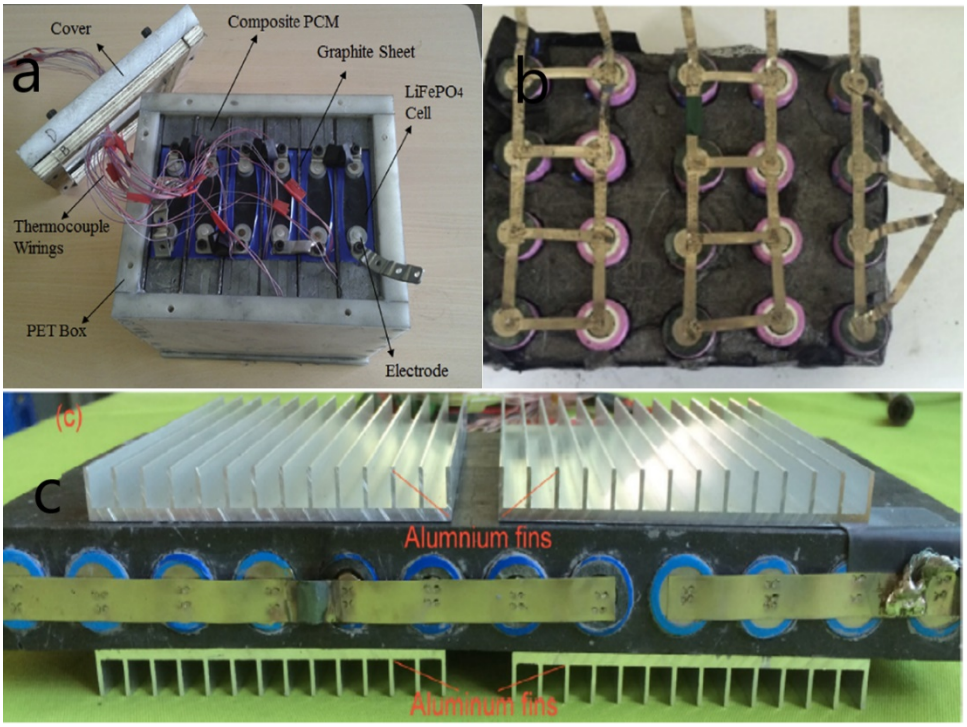

Figure 14 Various battery heat dissipation module contained EG/PCMs, a [110], b [126] and c [127] respectively.

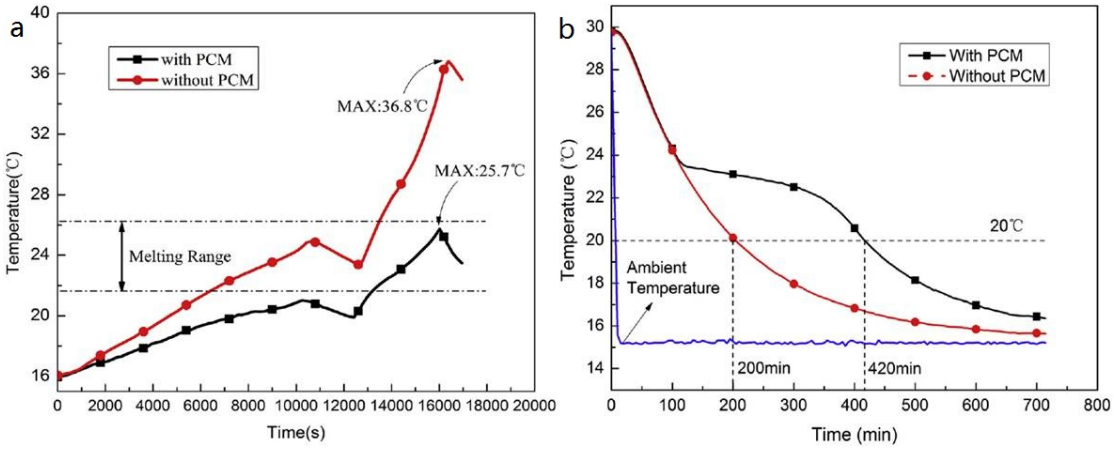

Figure 15 Experimental temperature response of the battery modules with and without EG/Paraffin composite PCM during mixed charge-discharge cycle (a) and warm-keeping effect test (b) [110].

Gao *et al.* [113] reported that the EG/paraffin composites filled in the heat sink effectively reduced the heating and cooling rates of the simulated electronic chip and prolongs the temperature-controlling time. And that, with the filling of the composite PCM in the heat sink, the temperature-controlling time of the chip at the heating powers of 15 and 20 W increases by 59% and 20%, respectively, which reduces the possibility of burning out of electronic chips due to sharp temperature rise and provides the protection of electronic devices.

6.2 Applications of EG/PCM composites in thermal energy storage

As mentioned, it is obvious that both heat storage time and retrieval time was reduced significantly for the EG/PCMs composites compared with those for PCMs without EG addition. As shown in Fig. 13b, for the EG (10)/AC (90) composite, the heat storage and retrieval durations in a LTES unit were reduced by 45% and 78%, respectively, compared with those of pure AC [47].

Lopez *et al.* reported an example of PCM application which illustrates the interest on EG/salt composites (uni-axial compression route) for high-temperature thermal energy storage purposes [114]. These composites allow the significant reduction in the storage system investment cost. A shell-and-tube storage system was considered. This system consisted of a block made of EG/salt materials with a two-phase heat transfer fluid (water/vapor) passing through a set of parallel tubes that crossed the block (Fig.16). For modeling purposes, identical conditions were assumed in all the tubes. The storage unit was assumed to be composed of parallel storage elements. Only a single pipe with surrounding storage material was calculated to reduce the computation time. The energy stored by the system was then the product of the number of tubes by the energy stored in only one of these units. The charging/discharging processes were assumed to be completed when the solid/liquid phase front between adjacent tubes touched each other. The PCM properties used in the analysis listed in Table 13, and results are included in Table 14. Using EG/salt composites, instead of salt, resulted in the significant reduction in the total tube length. This phenomenon is particularly interesting because the price of steel tubes represents a major part of the total cost of the storage system. Fig.17 shows estimated investment cost reduction resulting from EG/salt material utilization. As expected, the reduction cost is independent of the heat storage capacity, but is strongly dependent on power requirements. Considering the reduction in charging/discharging time, the use of EG/salt composites continues to attract much interest. In all cases, an optimal composition of the materials appeared at 10 wt% EG content. This characteristic resulted from a balance between the costs of the EG content and steel required to fit the design constraints. Liu *et al.* [128] reported that the heat storage time of the composites were 56.03%, 5.95%, 12.18% and 8.69% shorter than that of paraffin when the additives were EG (2.5 wt.%), graphene nanoplatelet (2.5 wt.%), GP (2.5 wt.%) and carbon nanotube (2.5 wt.%),

respectively, and the heat release time also decreased by 54.26%, 12.29%, 10.93% and 19.47%, respectively. As a result, EG can be considered as an effective heat diffusion promoter to enhance the heat transfer performance of paraffin compared to that of graphene nanoplatelet, GP and carbon nanotube.

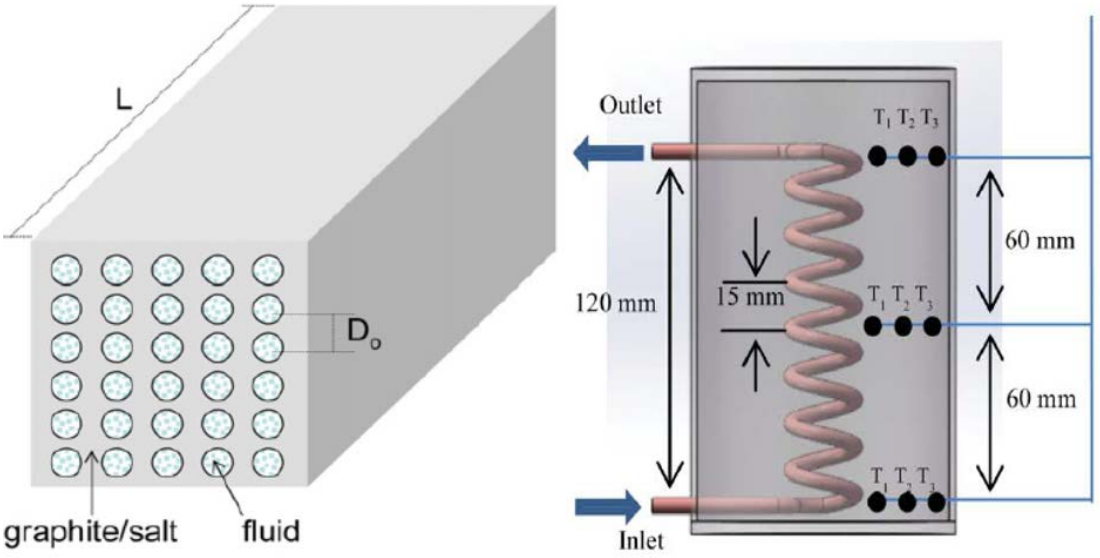

Figure 16 Sketch of a shell-and-tube [114] and a spiral copper pipe [128] storage system.

Table 13 Values of the PCM physical properties used in the analysis [114].

Salt properties	EG properties
Density = 2100 kg m^{-3}	Density = 2200 kg m^{-3} (true density)
Specific heat = 1822 J kg^{-1} K^{-1}	Specific heat = 712 J kg^{-1} K^{-1}
Melting temperature = 223 °C	
Latent heat = 106 kJ kg^{-1}	
Thermal conductivity values as a function of EG amount according to the measurements carried out in Ref. [72] 0 wt% EG: 1.2 W m^{-1} K^{-1}; 5 wt% EG: 2 W m^{-1} K^{-1}; 10 wt% EG: 10.5 W m^{-1} K^{-1}; 15 wt% EG: 20 W m^{-1} K^{-1}.	

Table 14 Results from pre-dimensioning of the storage systems. Internal tubes diameter is equal to 20 mm. The heat transfer fluid temperature is assumed to be 10 °C higher than the melting temperature of the salt. Convection heat transfer coefficient between the tubes wall and the fluid is 1000 W m^{-2} K^{-1}[114].

Storage capacity(kW h)	Charging time(h)	EG (wt%)	L_{tubes}(m)	D_o(m)	M_{salt}(kg)	M_{EG}(kg)
20	2	0	121.5	0.03	679.25	0
		5	90.1	0.08	679.25	35.8
		10	36.3	0.12	679.25	75.5
		15	27.8	0.14	679.25	119.9
	8	0	44.1	0.10	679.25	0
		5	31.5	0.13	679.25	35.8
		10	11.2	0.21	679.25	75.8
		15	8.1	0.26	679.25	119.9
100	2	0	607.5	0.06	3396.3	0
		5	450.5	0.08	3396.3	178.8
		10	181.4	0.12	3396.3	377.4
		15	138.9	0.14	3396.3	599.3

	8	0	220.5	0.10	3396.3	0
		5	157.5	0.13	3396.3	178.8
		10	55.8	0.21	3396.3	377.4
		15	40.5	0.26	3396.3	599.3
500	2	0	3037.5	0.06	16981.1	0
		5	2252.3	0.08	16981.1	893.7
		10	907.0	0.12	16981.1	1886.8
		15	694.5	0.14	16981.1	2996.7
	8	0	1102.7	0.10	16981.1	0
		5	787.2	0.13	16981.1	893.7
		10	278.8	0.21	16981.1	1886.8
		15	202.7	0.26	16981.1	2996.7

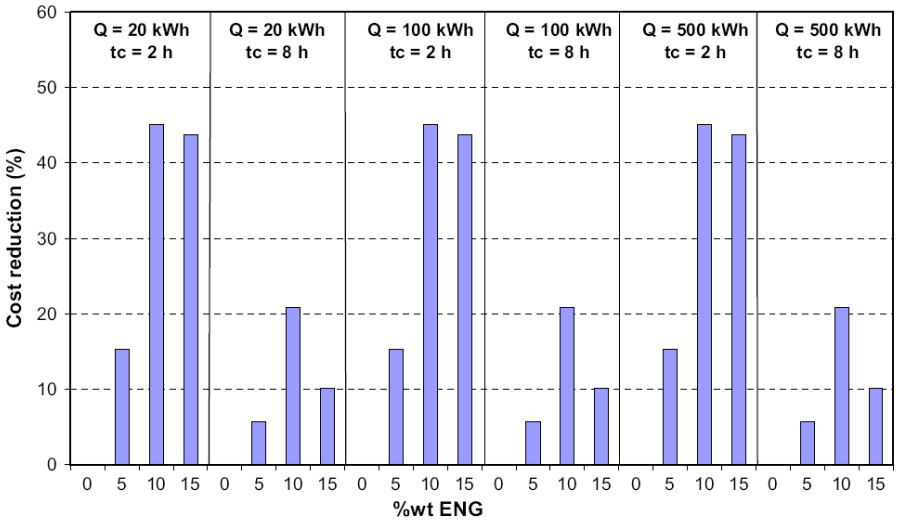

Figure 17 Investment cost reduction induced by thermal conductivity enhancement. Prices assumptions: 0.6 and 6€/kg for salt, and EG, respectively, and 25 €/m for steel 316L [114].

6.3 Applications of EG/PCM composites in buildings

Incorporating a suitable PCM into the walls, ceiling and floor of a building can function as reducing the room temperature swings in the building, thus leading to an improvement in the human comfort and a reduce in the energy consumption for the building [1]. TESCM was fabricated by integrating ordinary cement mortar with various mass ratios of EG/n-octadecane composite [103]. The mass fraction of n-octadecane in EG/n-octadecane composite is as large as 90%. Fig.18 shows the indoor temperature variation curves of the test rooms with the top boards containing the EG/n-octadecane composite with its mass percentage of 0, 0.5, 1.2, and 2.5%, respectively. From Fig.18, the indoor temperature variation curves gradually slow down with the increase in the mass percentage of the composite PCM in the top boards. Consequently, the test rooms with different top boards reach different indoor peak temperatures. It is revealed that the TESCM boards containing the EG/n-octadecane composite have a function of reducing energy consumption by decreasing the indoor temperature variation, and the function is enhanced with the increase in the mass ratio of the composite in the TESCM boards. It can be predicted that these kinds of TESCM containing the EG/n-octadecane composite have promising applications in buildings.

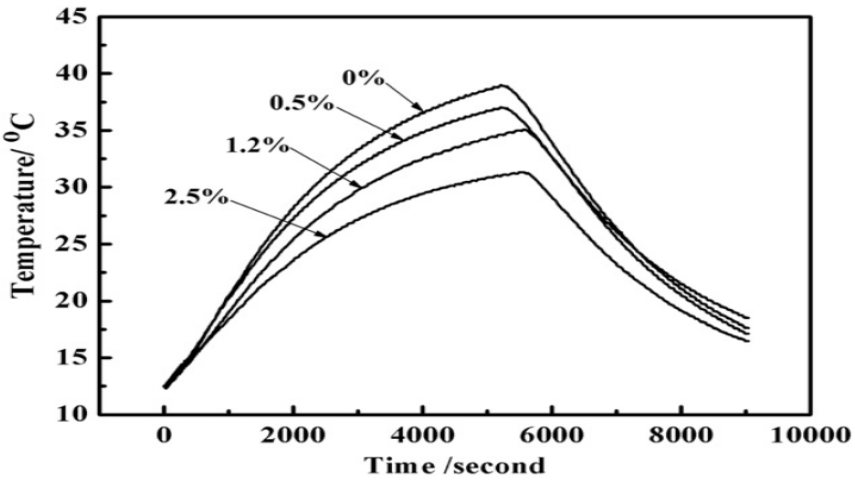

Figure 18 Indoor temperature variation curves of the test rooms with the top boards containing different mass percentages of the EG/n-octadecane composite [103].

The simulation room showed that the Electric radiant floor heating system (ERFHS) with PCM layer which composited of SAT, formamide and EG presented smaller indoor operative temperature fluctuation in vertical orientation and longer total thermal comfort time (12.65 h), which greatly exceeds that of the one without CPCM layer (1.836 h) [129].

7. Conclusion

A review of experimental/ computational studies to promote the thermal conductivity of PCMs using EG was presented. The information obtained was divided into five parts: heat transfer enhancement techniques, preparations, characterizations, simulations and application of the EG/PCM composites. Several methods that enhance the heat transfer in latent heat thermal storage systems were briefly introduced. The EG/PCM composites prepared using all kinds of preparation methods were described in detail. The thermophysical properties of the composites were characterized. Simulations and applications of EG/PCM composites also confirmed that using EG/PCM composites, compared with the pure PCMs, result in significant enhancement effects.

Acknowledgements

This paper was partially sponsored by the project 51666002 of the China National Natural Science Foundation, the project 2015BS0501 of the Inner Mongolia Natural Science Foundation and the project of 201702162 of Inner Mongolia Science and technology.

References

[1] Raj VAA, Velarj R. Review on free cooling of buildings using phase change materials. Renew Sustain Energ Rev 2010; 14: 2819-2829.
[2] Darkwa K, OCallaghan PW, Tetlow D. Phase-change drywalls in a passive-solar building. Appl Energ 2006; 83: 425-435.
[3] Yagi J, Akiyama T. Storage of thermal energy for effective use of waste heat from industries. J Mater Process Technol 1995; 48:793-804.
[4] Fok SC, Shen W, Tan FL. Cooling of portable hand-held electronic devices using phase change materials in finned heat sinks. Int J Therm Sci 2010; 49:109-117.
[5] Zalba B, Marin JM, Cabeza LF, Mehling H. Review on thermal energy storage with phase change: materials, heat transfer analysis and applications. Appl Therm Eng 2003; 23: 251-283.
[6] Farid MM, Khudhair AM, Razack SAK, Al-Hallaj S. A review on phase change energy storage: material and applications. Energ Convers Manage 2004; 45: 1597-1615.

[7] Sharma SD, Sagara K. Latent heat storage materials and systems: a review. Int J Green Energy 2005; 2: 1-56.
[8] Kenisarin M, Mahkamov K. Solar energy storage using phase change materials. Renew Sustain Energ Rev 2007; 11: 1913-1965.
[9] Regin AF, Solanki SC, Saini JS. Heat transfer characteristics of thermal energy storage system using PCM capsules: a review. Renew Sustain Energ Rev 2008; 12: 2438-2458.
[10] Jegadheeswaran S, Pohekar SD. Performance enhancement in latent heat thermal storage system: a review. Renew Sustain Energ Rev 2009; 13: 2225-2244.
[11] Fan LW, Khodadadi JM. Thermal conductivity enhancement of phase change materials for thermal energy storage: A review. Renew Sustain Energ Rev 2011; 15: 24-46.
[12] Abhat A, Aboul-Enein S, Malatidis N. Heat of fusion storage systems for solar heating applications, in: C. Den Quden (Ed.). Thermal Storage of Solar Energy, Martinus Nijhoff, 1981.
[13] Morcos VH. Investigation of a latent heat thermal energy storage system. Solar Wind Technol 1990; 7:197-202.
[14] Padmanabhan PV, Krishna Murthy MV. Outward phase change in a cylindrical annulus with axial fins on the inner tube. Int J Heat Mass Tran 1986; 29:1855-1868.
[15] Velraj R, Seeniraj RV, Hafner B, Faber C, Schwarzer K. Experimental analysis and numerical modeling of inward solidification on a finned vertical tube for a latent heat storage unit. Sol Energy 1997; 60: 281-290.
[16] Velraj R, Seeniraj RV, Hafner B, Faber C, Schwarzer K. Heat transfer enhancement in a latent heat storage system. Sol Energy 1999; 65:171-180.
[17] Ismail KAR, Alves CLF, Modesto MS. Numerical and experimental study on the solidification of PCM around a vertical axially finned isothermal cylinder. Appl Therm Eng 2001; 21: 53-77.
[18] Siegel R. Solidification of low conductivity material containing dispersed high conductivity particles. Int J Heat Mass Tran 1977; 20: 1087-1089.
[19] Tong X, Khan J, Amin MR. Enhancement of heat transfer by inserting a metal matrix into a phase change material. Numer Heat Tr A-Appl 1996; 30: 125-141.
[20] Boomsma K, Poulikakos D. On the effective thermal conductivity of a three-dimensionally structured fluid-saturated metal foam. Int J Heat Mass Tran 2001; 44:827-836.
[21] Zhong YJ, Guo QG, Li SZ, Shi JL, Liu L. Heat transfer enhancement of paraffin wax using graphite foam for thermal energy storage. Sol Energ Mat Sol C 2010; 94: 1011-1014.
[22] Fedden AD, Franke ME. Graphitized carbon foam with phase change material for thermal energy storage. AIAA Paper 2006; 3133.
[23] Harris RJ, Leland Q, Du JH, Chow LC. Characterization of paraffin-graphite foam and paraffin-aluminum foam thermal energy storage systems. AIAA Paper 2006; 3132.
[24] Sari A, Karaipekli A. Thermal conductivity and latent heat thermal energy storage characteristics of paraffin/ expanded graphite composite as phase change material. Appl Therm Eng 2007; 27: 1271-1277.
[25] Sari A, Karaipekli A. Preparation, thermal properties and thermal reliability of palmitic acid/expanded graphite composite as form-stable PCM for thermal energy storage. Sol Energ Mat Sol C 2009; 93: 571-576.
[26] Karaipekli A, Sari A, Kaygusuz K. Thermal conductivity improvement of stearic acid using expanded graphite and carbon fiber for energy storage applications. Renew Energ 2007; 32: 2201-2210.
[27] Zhao JG, Guo Y, Feng F, Tong QH, Qv WS, Wang HQ. Microstructure and thermal properties of a paraffin/expanded graphite phase-change composite for thermal storage. Renew Energ 2011; 36: 1339-1342.
[28] Fukai J, Kanou M, Kodama Y, Miyatake O. Thermal conductivity enhancement of energy storage media using carbon fibers. Energ Convers Manage 2000; 41: 1543-1556.
[29] Fukai J, Hamada YC, Morozumi Y, Miyatake O. Effect of carbon-fiber brushes on conductive heat transfer in phase change materials. Int J Heat Mass Tran 2002; 45: 4781-4792.
[30] Fukai J, Morozumi Y, Hamada Y, Miyatake O. Transient response of thermal energy storage unit using carbon fibers as thermal conductivity promoter. Proceedings of the 3rd European Thermal Sciences Conference, Pisa (Italy), 2000.
[31] Cheng WL, Zhang RM, Xie K, Liu N, Wang J. Heat conduction enhanced shape-stabilized paraffin/HDPE composite PCMs by graphite addition: Preparation and thermal properties. Sol Energ Mat Sol C 2010; 94:1636-1642.
[32] Wang XL, Guo QG, Wang JZ, Zhong YJ, Wang LY, Wei XH, Liu L. Thermal conductivity enhancement of form-stable phase-change composites by milling of expanded graphite, micro-capsules and polyethylene. Renew Energ 2013; 60: 506-509.

[33] Wei XH, Liu L, Zhang JX, Shi JL, Guo QG. Synthesis of HClO4-GICs and the performance of flexible graphite produced from them. New Carbon Mater (China) 2007; 22: 342-348.
[34] Fukushima H. Graphite nanoreinforcements in polymer nanocomposites. Ph.D Thesis, Michigan State University, East Lansing, MI, USA, 2003.
[35] Xia L, Zhang P, Wang RZ. Preparation and thermal characterization of expanded graphite/ paraffin composite phase change material. Carbon 2010; 48:2538-2548.
[36] Pincemin S, Py X, Olives R, Christ M, Oettinger O. Elaboration of conductive thermal storage composites made of phase change materials and graphite for solar plant. J Sol Energ-T ASME 2008; 130:011005.
[37] Inagaki M, Nagata T, Suwa T, Toyoda M. Sorption kinetics of various oils onto exfoliated graphite. New Carbon Mater 2006; 21: 98-102.
[38] Xiao JB, Huang J, Zhu PP, Wang CH, Li XX. Preparation, characterization and thermal properties of binary nitrate salts/expanded graphite as composite phase change material. Thermochim Acta 2014; 587:52-58.
[39] Li YF, Zhang D. Thermal conductivity anisotropy of expanded graphite/ LiCl-NaCl phase change material. J Funct Mater (China) 2013; 16:2409-2415.
[40] Zhang T, Zeng L, Zhang D. Improvement of thermal properties of hybrid inorganic salt phase change materials by expanded graphite and graphene. Inorg Chem Ind 2010; 42: 24-26.
[41] Zhong LM, Zhang XW, Luan Y, Wang G, Feng YH, et al. Preparation and thermal properties of porous heterogeneous composite phase change materials based on molten salts/expanded graphite. Sol Energy 2014; 107: 63-73.
[42] Li YF, Zhang D. Study on high temperature phase change composites of NaNO3-KNO3/ expanded graphite by saturated water solution method. J Funct Mater 2013; 10:1451-1456.
[43] Wang CY, Feng LL, Wei L, Zheng J, Tian WH, Li XG. Shape-stabilized phase change materials based on polyethylene glycol/ porous carbon composite: The influence of the pore structure of the carbon materials. Sol Energ Mat Sol C 2012; 105: 21-26.
[44] Zeng JL, Gan J, Zhu FR, Yu SB, Xiao ZL, et al. Tetradecanol/expanded graphite composite form-stable phase change material for thermal energy storage. Sol Energ Mat Sol C 2014; 127: 122-128.
[45] Xiang JL, Lawrence TD. Investigation of exfoliated graphite nanoplatelets (xGnP) in improving thermal conductivity of paraffin wax-based phase change material. Sol Energ Mat Sol C 2011; 95: 1811-1818.
[46] Kang D, Xi P, Duan YQ, Gu XH, et al. Study on polyethylene glyol/ expanded graphite phase change composites for thermal storage. New Chem Mater 2011; 39(3): 106-109.
[47] Xia L, Zhang P. Thermal property measurement and heat transfer analysis of acetamide and acetamide/expanded graphite composite phase change material for solar heat storage. Sol Energ Mat Sol C 2011; 95: 2246-2254.
[48] Huang ZW, Gao XN, Xu T, Fang YT, et al. Thermal property measurement and heat storage analysis of LiNO3/KCl -expanded graphite composite phase change material. Appl Energ 2014; 115: 265-271.
[49] Fang GY, Li H, Chen Z, Liu X. Preparation and characterization of stearic acid/expanded graphite composites as thermal energy storage materials. Energy. 2010; 35:4622-4626.
[50] Li H, Liu X, Fang GY. Synthesis and characteristics of form-stable n-octadecane/expanded graphite composite phase change materials. Appl Phys A-Mater 2010; 100:1143-1148.
[51] Yang XJ, Yuan YP, Zhang N, Cao XL, Liu C. Preparation and properties of myristic-palmitic-stearic acid/expanded graphite composites as phase change materials for energy storage. Sol Energy 2014; 99:259-266.
[52] Huang J, Wang TY, Wang CH, Rao ZH. Exfoliated graphite/paraffin nanocomposites as phase change materials for thermal energy storage application. Mater Res Innov 2011; 15(6): 422-427.
[53] Hu XD, Gao XN, Li DL, Chen ST. Performance of paraffin/ expanded graphite composite phase change materials. CIESC Journal. 2013:64; 3831-3837.
[54] Sumin K, Lawrence TD. High latent heat storage and high thermal conductive phase change materials using exfoliated graphite nanoplatelets. Sol Energ Mat Sol C 2009; 93:136-142.
[55] Zhang ZG, Fang XM. Study on paraffin/expanded graphite composite phase change thermal energy storage material. Energ Convers Manage 2006; 47: 303-310.
[56] Zhou D, Zhao CY. Experimental investigations on heat transfer in phase change materials (PCMs) embedded in porous materials. Appl Therm Eng 2011; 31:970-977.
[57] Zhao CY, Zhou D, Wu ZG. Heat transfer of phase change materials (PCMs) in porous materials. Front Energy 2011; 5(2):174-180.

[58] Zhang N, Yuan YP, Du YX, Cao XL, et al. Preparation and properties of palmitic-stearic acid eutectic mixture/expanded graphite composite as phase change material for energy storage. Energy 2014; 78:950-956.
[59] Yuan YG, Yuan YP, Zhang N, Du YX, Cao XL. Preparation and thermal characterization of capric–myristic–palmitic acid/expanded graphite composite as phase change material for energy storage. Mater Lett 2014; 125:154-157.
[60] Zhang N, Yuan YP, Wang X, Cao XL, et al. Preparation and characterization of lauric-myristic-palmitic acid ternary eutectic mixtures/expanded graphite composite phase change material for thermal energy storage. Chem Eng J 2013; 231:214-219.
[61] Sari A, Karaipekli A, Kaygusuz K. Fatty acid/expanded graphite composites as phase change material for latent heat thermal energy storage. Energ Source Part A 2008; 30: 464-474.
[62] Ma F, Li Y, Cheng LY, Chen MH. Preparation and properties of octadecane-palmitic acid/expanded graphite phase change energy storage materials. J Aeronaut Mater (China) 2010; 30(3): 66-69.
[63] Zhou JH, Zhang L, Shen XL. Studies on properties of nano-SiO2/silicone modified polyacrylate composite. J Funct Mater (China) 2010; 41(suppl): 180-183.
[64] Wu QS, Qiu Y, Li SP, Zhu HJ. Study of capric acid and hexadecanol/expanded graphite composite as phase change material for thermal energy storage. J Build Mater (China) 2014; 17(1):84-88.
[65] James H, Shane A, Robert J, Framingham A, Raymond A. Flexible graphite material of expanded particles compressed together, US Patent 3404061, 1968.
[66] Py X, Olives R, Mauran S. Paraffin/ porous-graphite-matrix composite as a high and constant power thermal storage material. Int J Heat Mass Tran 2001; 44:2727-2737.
[67] Mills A, Farid M, Selman JR, Al-Hallaj S. Thermal conductivity enhancement of phase change materials using a graphite matrix. Appl Therm Eng 2006; 26:1652-1661.
[68] Zhao JG, Guo QG, Liu L, Wei XH, Zhang JX. Polyethylene glycol/expanded graphite phase change composites for thermal storage. Mod Chem Ind (China) 2008; 28(9): 46-47.
[69] Zhong YJ, Li SZ, Wei XH, Liu ZJ, Guo QG, et al. Heat transfer enhancement of paraffin wax using compressed expanded natural graphite for thermal energy storage. Carbon 2010; 48: 300-304.
[70] Zhong YJ, Guo QG, Li L, Wang XL, et al. Heat transfer improvement of Wood's alloy using compressed expanded natural graphite for thermal energy storage. Sol Energ Mat Sol C 2012, 100: 263-267.
[71] Wang XL, Guo QG, Zhong YJ, Wei XH, et al. Heat transfer enhancement of neopentyl glycol using compressed expanded natural graphite for thermal energy storage. Renew Energ 2013; 51: 241-246.
[72] Zoubir A, Jéréme L, Elena PDB. KNO3/NaNO3 –Graphite materials for thermal energy storage at high temperature: PartI.- Elaboration methods and thermal properties. Appl Therm Eng 2010; 30:1580-1585.
[73] Couto Aktay K S, Tamme R, Müller-Steinhagen H. Thermal Conductivity of High-Temperature Multicomponent Materials with Phase Change. Int J Thermophys 2008; 29: 678-692.
[74] Wang SP, Qin P, Fang XM, Zhang ZG, Wang SF, et al. A novel sebacic acid/expanded graphite composite phase change material for solar thermal medium-temperature applications. Sol Energy 2014; 99:283-290.
[75] Ling ZY, Chen JJ, Xu T, Fang XM, et al. Thermal conductivity of an organic phase change material/expanded graphite composite across the phase change temperature range and a novel thermal conductivity model. Energ Convers Manage 2015; 102: 202-208.
[76] Inaba H, Tu P. Evaluation of thermophysical characteristics on shape-stabilized paraffin as a solid-liquid phase change material. Heat Mass Transfer 1997; 32: 307-312.
[77] Sari A. Form-stable paraffin/high density polyethylene composites as solid-liquid phase change material for thermal energy storage: preparation and thermal properties. Energ Convers Manage 2004; 45: 2033-2042.
[78] Cheng WL, Liu N, Wu WF. Studies on thermal properties and thermal control effectiveness of a new shape-stabilized phase change material with high thermal conductivity. Appl Therm Eng 2012; 36:345-352.
[79] Almaadeed M.A, Labidi S, Krupa I, Karkri M. Effect of expanded graphite on the phase change materials of high density polyethylene/wax blends. Thermochim Acta 2015; 600:35-44.
[80] Wang XL, Guo QG, Wang LY, Wei XH, et al. Thermal conductivity enhancement of form-stable HDPE/ paraffin by expanded graphite addition. J Funct Mater 2013; 23: 3401-3404.
[81] Zhang P, Hu Y, Song L, Ni JX, Xing WY, Wang J. Effect of expanded graphite on properties of high-density polyethylene/ paraffin composite with intumescent flame retardant as a shape-stabilized phase change material. Sol Energ Mat Sol C 2010; 94: 360-365.

[82] Zhang P, Song L, Lu HD, Wang J, Hu Y. The influence of expanded graphite on thermal properties for paraffin/ high density polyethylene/ chlorinated paraffin/antimony trioxide as a flame retardant phase change material. Energ Convers Manage 2010; 51: 2733-2737.
[83] Sittisart P, Farid MM. Fire retardants for phase change materials. Appl Energ 2011; 88: 3140-3145.
[84] Cai YB, Wei QF, Huang FL, Lin SL, et al. Thermal stability, latent heat and flame retardant properties of the thermal energy storage phase change materials based on paraffin/high density polyethylene composites. Renew Energ 2009; 34: 2117-2123.
[85] Mhike W, Focke WW, Mofokeng JP, Luyt AS. Thermally conductive phase change materials for energy storage based on low-density polyethylene, soft Fischer Tropsch wax and graphite. Thermochim Acta 2012; 527: 75-82.
[86] Zhang XM, Deng PF, Feng RX, Song J. Novel gelatinous shape-stabilized phase change materials with high heat storage density. Sol Energ Mat Sol C 2011; 95: 1213-1218.
[87] Xiao M, Feng B, Gong K. Thermal performance of a high conductive shape stabilized thermal storage material. Sol Energ Mat Sol C 2001; 69: 293-296.
[88] Xiao M, Feng B, Gong K. Preparation and performance of shape stabilized phase change thermal storage materials with high thermal conductivity. Energ Convers Manage 2002; 43: 103-108.
[89] Mochane M.J, Luyt A.S. Synergistic effect of expanded graphite, diammonium phosphate and Cloisite 15A on flame retardant properties of EVA and EVA/wax phase-change blends. J Mater Sci 2015; 50:3485-3494.
[90] Mochane M.J, Luyt A.S. The Effect of Expanded Graphite on the Thermal Stability, Latent Heat, and Flammability Properties of EVA/Wax Phase Change Blends. Polym Eng Sci 2015; 55(6): 1255-1262.
[91] Mochane M.J, Luyt A.S. The Effect of Expanded Graphite on the Physical Properties of Conductive EVA/Wax Phase Change Blends for Thermal Energy Storage. Polym Composite 2016; 37(10): 3025-3032.
[92] Li M, Wu ZS. Preparation and performance of highly conductive phase change materials prepared with paraffin, expanded graphite, and diatomite. Int J Green Energy 2011; 8: 121-129.
[93] Kao HT, Li M, Lv XW, Tan JM. Preparation and thermal properties of expanded graphite/paraffin/organic montmorillonite composite phase change material. J Therm Anal Calorim 2012; 107: 299-303.
[94] Shin HK, Park M, Kim HY, Park SJ. Thermal property and latent heat energy storage behavior of sodium acetate trihydrate composites containing expanded graphite and carboxymethyl cellulose for phase change materials. Appl Therm Eng 2015; 75: 978-983.
[95] Duan ZJ, Zhang HZ, Sun LX, Cao Z, et al. CaCl2-6H2O/Expanded graphite composite as form-stable phase change materials for thermal energy storage. J Therm Anal Calorim 2014; 115:111-117.
[96] Li JL, Xue P, Ding WY, Han JM, Sun GL. Micro-encapsulated paraffin/ high-density polyethylene/ wood flour composite as form-stable phase change material for thermal energy storage. Sol Energ Mat Sol C 2009; 93: 1761-1767.
[97] Jeong SG, Chang SJ, We S, Kim S. Energy efficient thermal storage montmorillonite with phase change material containing exfoliated graphite nanoplatelets. Sol Energ Mat Sol C 2015; 139: 65-70.
[98] Cai YB, Gao CT, Zhang T, Zhang Z, et al. Influences of expanded graphite on structural morphology and thermal performance of composite phase change materials consisting of fatty acid eutectics and electrospun PA6 nanofibrous mats. Renew Energ 2013; 57: 163-170.
[99] Zhang L, Zhu JQ, Zhou WB, Wang J, Wang Y. Thermal and electrical conductivity enhancement of graphite nanoplatelets on form-stable polyethylene glycol/polymethyl methacrylate composite phase change materials. Energy 2012; 39: 294-302.
[100] Zeng JL, Zheng SH, Yu SB, Zhu FY, et al. Preparation and thermal properties of palmitic acid/polyaniline/exfoliated graphite nanoplatelets form-stable phase change materials. Appl Energ 2014; 115: 603-609.
[101] Li M, Wu ZS, Tan JM. Properties of form-stable paraffin/silicon dioxide/expanded graphite phase change composites prepared by sol-gel method. Appl Energ 2012; 92: 456-461.
[102] Li W, Zhang R, Jiang N, Tang XF, et al. Composite macrocapsule of phase change materials/expanded graphite for thermal energy storage. Energy 2013; 57: 607-614.
[103] Zhang ZG, Shi GQ, Wang SP, Fang XM, Liu XH. Thermal energy storage cement mortar containing n-octadecane/expanded graphite composite phase change material. Renew Energ 2013; 50: 670-675.
[104] Alrashan A, Mayyas A. T, Al-Hallaj S. Thermo-mechanical behaviors of the expanded graphite-phase change material matrix used for thermal management of Li-ion battery packs. J Mater Process Tech 2010; 210(1): 174-179.

[105] Liu X, Shao P, Yang Y. Thermal expansion pressure test of paraffin-expanded graphite composite phase change materials under constraint. J Lanzhou University (Natural Sciences) 2012; 48(2): 122-126.
[106] Yvan D, Daniel RR, Nizar BS, Stéphane L, et al. A review on phase-change materials: mathematical modeling and simulations. Renew Sustain Energ Rev 2011; 15: 112-130.
[107] Lu XW, Kao HT, Li M. Thermal analysis in phase transition process of expanded graphite/ paraffin wax composite phase change materials. Materials Review B (China): 2011; 25: 131- 134.
[108] Pincemin S, Olives R, Py X, Christ M. Highly conductive composites made of phase change materials and graphite for thermal storage. Sol Energ Mat Sol C 2008; 92: 603-613.
[109] Andrew M, Said AH. Simulation of passive thermal management system for lithium-ion battery packs. J Power Sources 2005; 141: 307-315.
[110] Lin CJ, Xu SC, Chang GF, Liu JL. Experiment and simulation of a LiFePO4 battery pack with a passive thermal management system using composite phase change material and graphite sheets. J Power Sources 2015; 275: 742-749.
[111] Wang XL, Guo QG, Zhong YJ, Wang LY, et al. Numerical simulation of the effect of heat conductive fillers on the heat conduction behavior of paraffin phase change energy storage system. New Carbon Materials (China) 2014; 29: 0149-0155.
[112] Luo JF, Yin HW, Li WY, Xu ZJ, Shao ZZ, et al. Numerical and experimental study on the heat transfer properties of the composite paraffin/expanded graphite phase change material. Int J Heat Mass Tran 2015; 84: 237-244.
[113] Gao XN, Li DL, Sun T, Cao X, He WX. Performance of temperature-controlled electronic heat sink with composite paraffin/expanded graphite phase change material. Journal of south china university of technology 2012; 40(1): 7-12.
[114] Jérôme L, Zoubir A, Elena PDB. KNO3/ NaNO3- Graphite materials for thermal energy storage at high temperature: Part II. –Phase transition properties. Appl Therm Eng 2010, 30: 1586-1593.
[115] Li WW, Cheng WL, Xie B, Liu N, Zhang LS. Thermal sensitive flexible phase change materials with high thermal conductivity for thermal energy storage. Energ Convers Manage 2017; 149: 1-12.
[116] Yuan YP, Zhang N, Li TY, Cao XL, Long WY. Thermal performance enhancement of palmitic-stearic acid by adding graphene nanoplatelets and expanded graphite for thermal energy storage: A comparative study. Energy 2016; 97: 488-497.
[117] He JS, Yang XQ, Zhang GQ, A phase change material with enhanced thermal conductivity and secondary heat dissipation capability by introducing a binary thermal conductive skeleton for battery thermal management. Appl Therm Eng 2019; 148: 984-991.
[118] Tao ZC, Wang HB, Liu JQ, Zhao WG, Liu ZJ, Guo QG. Dual-level packaged phase change materials -thermal conductivity and mechanical properties. Sol Energ Mat Sol C 2017; 169: 222-225.
[119] Wang TY, Wang SF, Geng LX, Fang YT. Enhancement on thermal properties of paraffin/calcium carbonate phase change microcapsules with carbon network. Appl Energ 2016; 179: 601-608.
[120] Zhang SL, Wu W, Wang SF. Experimental investigations of Alum/expanded graphite composite phase change material for thermal energy storage and its compatibility with metals. Energy 2018; 161: 508-516.
[121] Angelo G, Jiang X. A coupled thermal and electrochemical study of lithium-ion battery cooled by paraffin/porous-graphite-matrix composite. J Power Sources 2016; 315: 127-139.
[122] Ling ZY, Cao JH, Zhang WB, Zhang ZG, Gao XN. Compact liquid cooling strategy with phase change materials for Li-ion batteries optimized using response surface methodology. Appl Energ 2018; 228: 777-788.
[123] Huang X，Alva G, Liu LK, Fang GY. Preparation, characterization and thermal properties of fatty acid eutectics/bentonite/expanded graphite composites as novel form–stable thermal energy storage materials. Sol Energ Mat Sol C 2017; 166: 157-166.
[124] Huang ZW, Zhai DH, Gao XN, Xu T, Fang YT, Zhang ZG. Theoretical study on effective thermal conductivity of salt/expanded graphite composite material by using fractal method. Appl Therm Eng 2015; 86: 309-317.
[125] Wang ZY, Li XX, Zhang GQ, Lv YF, Wang C, He FQ, Yang CZ, Yang CX. Thermal management investigation for lithium-ion battery module with different phase change materials. RSC Adv 2017; 7: 42909-42918.
[126] Ling ZY, Wen XY, Zhang ZG, Fang XM, Gao XN. Thermal management performance of phase change materials with different thermal conductivities for Li-ion battery packs operated at low temperatures. Energy 2018; 144: 977-983.

[127] Lv YF, Yang XQ, Li XX, Zhang GQ, Wang ZY, Yang CZ. Experimental study on a novel battery thermal management technology based on low density polyethylene-enhanced composite phase change materials coupled with low fins. Appl Energ 2016; 178: 376-382.
[128] Liu CZ, Zhang X, Lv PZ, Li YM, Rao ZH. Experimental study on the phase change and thermal properties of paraffin/carbon materials based thermal energy storage materials. Phase Transitions: A Multinational Journal 2017; 90(7): 717-731.
[129] Fang YT, Ding YF, Tang YF, Liang XH, Jin C, Wang SF, Gao XN, Zhang ZG. Thermal properties enhancement and application of a novel sodium acetate trihydrate-formamide/expanded graphite shape-stabilized composite phase change material for electric radiant floor heating. Appl Therm Eng 2019; 150: 1177-1185.